RM E53D24

NACA

RESEARCH MEMORANDUM

NACA RM E53D24

INVESTIGATION OF AN AXIAL-FLOW-COMPRESSOR ROTOR WITH CIRCULAR-ARC BLADES OPERATING UP TO A ROTOR-INLET RELATIVE MACH NUMBER OF 1.22

By William H. Robbins and Frederick W. Glaser

Lewis Flight Propulsion Laboratory
Cleveland, Ohio

NATIONAL ADVISORY COMMITTEE
FOR AERONAUTICS

WASHINGTON

July 3, 1953

NATIONAL ADVISORY COMMITTEE FOR AERONAUTICS

RESEARCH MEMORANDUM

INVESTIGATION OF AN AXIAL-FLOW-COMPRESSOR ROTOR WITH CIRCULAR-ARC BLADES OPERATING UP TO A ROTOR-INLET RELATIVE MACH NUMBER OF 1.22

By William H. Robbins and Frederick W. Glaser

SUMMARY

A 14-inch-diameter axial-flow-compressor rotor with a hub-tip diameter ratio of 0.50 was designed and operated to investigate the blade-element characteristics as well as the over-all performance of a set of circular-arc rotor blades operating over a range of inlet relative Mach number from 0.40 to 0.82 with the inlet guide vanes installed and from 0.44 to 1.22 with the guide vanes removed. At design tip speed of 1120 feet per second, a peak pressure ratio of 1.277 was reached at an efficiency of 0.85 and an equivalent weight flow of 23.75 pounds per second for the rotor with guide vanes. A maximum design-speed efficiency of 0.905 was obtained at a weight flow of 28.18 and a pressure ratio of 1.186. At an equivalent tip speed of 1000 feet per second, which was considered to be the best operating speed for the rotor without guide vanes, a peak pressure ratio of 1.297 was reached at an equivalent weight flow of 32.30 pounds per second and an efficiency of 0.89. A peak efficiency of 0.895 was reached at an equivalent weight flow of 33.60 pounds per second and a pressure ratio of 1.276.

In both investigations, it was possible to operate over a wide range of incidence angle at all radial positions with no large losses except at the blade tip. The optimum incidence angle appeared to increase as Mach number increased. At the design angle of incidence, the design turning-angle rule predicts accurately the turning at all radial positions except the hub section. At the hub, slight underturning resulted. In addition, the turning angle was not affected by Mach number over the range of Mach number investigated.

The design assumption of simple radial equilibrium proved to be relatively accurate, in that reasonably good checks of calculated and measured axial velocity were obtained. However, when the entropy-gradient term was included in the radial equilibrium calculation, there was better agreement between the measured data and calculated values of axial velocity.

[redacted]

In the rotor without guide vanes, at a tip speed of 1120 feet per second there were indications that the limiting relative Mach number, which was determined to be between 1.10 and 1.20, had been exceeded. Therefore, the over-all peak efficiency was reduced approximately 7 percent in this range of Mach number.

INTRODUCTION

In order to improve the performance of the axial-flow-compressor component of aircraft gas-turbine power plants, efforts are being made to decrease its size and weight (for a constant mass flow) without sacrificing its inherently high efficiency. Therefore, compressor designs are desirable which utilize high pressure ratio per stage and high weight flow per unit frontal area without sacrifice to compressor efficiency and range of efficient weight flow. It is possible to increase the axial velocity (which represents a gain in weight flow per unit frontal area) and the compressor pressure ratio, if the relative entrance compressor Mach number can be increased without incurring serious internal flow losses.

Most commercial compressor designs incorporate conventional subsonic compressor blading that is limited to relatively low Mach numbers (up to approximately 0.75) because of the complications that arise as the local velocities on the blade surfaces approach the speed of sound. In an effort to find an airfoil with a profile shape suitable for efficient operation at higher inlet Mach numbers, some two-dimensional cascade data were obtained on numerous airfoils with various profile shapes (ref. 1). The cascade results indicate that a circular-arc airfoil appears promising at high subsonic Mach numbers. The airfoil consists of circular-arc pressure and suction surfaces of different radii. The camber and thickness may be adjusted to any prescribed value by changing the radius of the pressure-surface or the suction-surface arcs, or both.

In view of these results (ref. 1), an axial-flow-compressor rotor with circular-arc blades was designed to operate at a relative inlet Mach number of approximately 0.8, and an investigation was made to determine the range of conditions over which the circular-arc airfoil would operate satisfactorily, as well as the three-dimensional flow effects on the performance of the rotor. In addition, the validity of the velocity-diagram procedure used in the design was determined.

The results of reference 2 indicate that an axial-flow-compressor rotor with similar blading could be operated efficiently at transonic Mach numbers (0.8 to 1.1). Since the rotor described in reference 2 had a lower aspect ratio and a higher solidity than those normally associated with commercial compressor designs, the present rotor blade design, which has conventional aspect ratio and solidity, was investigated up

to Mach numbers in the transonic range by removing the sheet-metal inlet guide vanes. The present report, therefore, discusses the performance of the circular-arc blade rotor operating over a range of Mach number with the inlet guide vanes installed and with the guide vanes removed.

COMPRESSOR DESIGN

Velocity-Diagram Calculation

Since the highest Mach number in an axial-flow compressor usually occurs at the compressor inlet, the design was made for a typical inlet stage (hub-tip diameter ratio, 0.50). Reference 3 was used as the basis for choosing the design velocity distributions. Results of the analyses of reference 3 indicate that a "wheel-plus-vortex" design (a design that establishes a wheel-type rotation through the guide vanes and a vortex or constant energy addition radially through the rotor) results in a design point with high pressure ratio and high mass flow for a given rotor relative Mach number limitation (M_1' approximately equal to 0.8). The velocity diagrams were calculated on the basis of the following assumptions:

1. Constant tip diameter (r_T = 14 in.)

2. Constant total enthalpy from hub to tip

3. Simple radial equilibrium of pressure and no radial flow $\left(\frac{1}{\rho}\frac{dp}{dr} = \frac{V_\theta^2}{r}\right)$

4. Rotor efficiency equal to 0.90

5. Wheel-type rotation through inlet guide vanes ($V_\theta = Kr$)

6. Constant or vortex energy addition through rotor ($V_{\theta,1} - V_{\theta,2} = K/r$)

7. Rotor Mach number limit M_1' equal to approximately 0.8

The rotor (when operating with inlet guide vanes) selected for this investigation had a design equivalent tip speed of 1120 feet per second and a design total-pressure ratio of 1.227 at an equivalent weight flow of 28.08 pounds per second. No area allowance was made for flow blockage caused by boundary-layer growth. Typical design velocity diagrams are shown in figure 1. The rotor in operation without inlet guide vanes

does not have any specific design point, because it was not designed to operate under these conditions. However, the knowledge of the effects of operation at transonic relative Mach numbers to be gained by removal of the guide vanes was considered to be of sufficient importance to warrant the investigation, even though it would be necessary to tolerate a large variation of incidence angle from hub to tip.

Blade Design

The guide vanes were 0.060-inch-thick sheet-metal blades having a circular-arc camber line with constant radius of curvature. The desired turning-angle distribution was obtained by varying the chord length from hub to tip. The guide vanes were designed on the basis of reference 4 in conjunction with reference 5. The guide-vane geometry is presented in table I.

A typical rotor blade section is shown in figure 2. Since complete cascade data on the circular-arc airfoil covering a range of solidities and inlet flow angles were not available, blade cambers and blade-angle settings were determined from an empirical deviation-angle rule described in reference 6. The deviation angle determined from this rule for circular-arc camber lines is given by:

$$\Delta = m\varphi\sqrt{1/\sigma} \tag{1}$$

The symbols used in this report are presented in the appendix. This equation, which was derived for two-dimensional cascades, is valid only for nominal incidence angle, which is defined as the incidence angle where the turning angle is 0.8 of its maximum or stall value. Since deviation angle varies only slightly with incidence angle in the stall-free range of the blade, this rule was applied in this design at an incidence angle of 2°, which was chosen on the basis of reference 1 to be the incidence angle for minimum drag. The incidence angle for minimum drag is termed optimum incidence angle throughout this report. A trial-and-error solution of equation (1) was necessary to compute the required camber angle and blade-setting angle from the specified turning angle and angle of incidence. The blade maximum thickness varied from 10 percent of chord at the hub to 5 percent at the tip. The chord length was 1.50 inches. The rotor blade geometry is presented in table II.

APPARATUS, INSTRUMENTATION, AND PROCEDURE

Compressor Installation

A schematic diagram of the compressor installation is shown in figure 3. Power was supplied to the compressor by a 1500-horsepower

dynamometer through a speed-increaser gearbox. Room air was drawn through a thin-plate sharp-edged orifice into an orifice tank. It then passed into a depression tank and into the compressor through a bell-mouth at the depression-tank exit. The air passed from the compressor into a collector and was discharged into the laboratory altitude exhaust system.

Instrumentation

Air flow through the compressor was measured by means of the sharp-edged, thin-plate orifice. The pressure drop across the orifice was indicated on a U-tube water manometer, and the room temperature was measured by means of four thermocouples located just ahead of the orifice tank.

Measuring station 0, which is shown in figure 4, was located in the depression tank. Temperatures in the tank were measured by three bare-wire thermocouples. Four wall taps were used to measure pressure. Since the air velocities in the depression tank were very low, measured pressures and temperatures were taken to be stagnation values.

Station 1 was located 1/2 inch behind the guide vanes. Preliminary circumferential surveys of total pressure were taken behind the guide vanes in order to find the position of the guide-vane wakes and the magnitude of the associated losses. Radial surveys of total pressure, static pressure, and flow angle were then made in the wake-free region of the annulus at five equally spaced points. In addition, wall static-pressure taps were provided at the compressor tip. The total temperature at station 1 was assumed to be equal to the depression-tank total temperature. When the guide vanes were removed, no surveys were taken at station 1. Inlet conditions were determined from the wall static taps and the depression-tank pressure and temperature measurements.

Station 2 was located 1/2 inch behind the rotor blades. In preliminary runs, it was noted that the inlet-guide-vane wakes could be picked up behind the rotor row. Because these guide-vane wakes extended over a large portion of the circumference at the station behind the rotor, it was impossible to locate the instrumentation so as to completely avoid measuring in these regions. The indications were, however, that the wakes had mixed sufficiently so that there were no large circumferential gradients of flow behind the rotor due to the guide-vane wakes. Therefore, it is believed that the data taken at station 2 represent the combined performance of the inlet guide vanes and the rotor row, even though complete circumferential surveys over a guide-vane passage were not taken at this station. The measurements taken at station 2 were radial surveys of total pressure, static pressure, and flow angle. In addition, three five-tip spike-type thermocouple rakes

were placed at three circumferential positions in the compressor casing. These thermocouples were connected so that it was possible to read the temperature difference between the depression tank and station 2. Each thermocouple could also be read individually in absolute units. Four wall static-pressure taps were provided on both the inner and outer walls. It was necessary to place the hub static taps approximately $1\frac{1}{2}$ inches behind station 2 because of the rotating hub. A summary of the instrumentation is given in table III. Photographs of the instrumentation are shown in figure 5.

The static-pressure probes and thermocouple rakes used in this investigation were calibrated for the effect of Mach number (over a range from 0.1 to 0.9) before installation in the test rig. This calibration covered the range of absolute Mach number that was encountered in this investigation. There were slight circumferential variations in static pressure and total temperature in the wake-free regions of the blade both before and after the rotor; however, they were not considered serious enough to warrant taking complete circumferential surveys at all data points. Some of these variations might be caused by the inlet bearing support struts and possible distortions in inlet flow.

Test Procedure

The investigation was divided into two phases: (1) rotor with guide vanes and (2) rotor alone. Data were taken at constant values of equivalent rotor speed $U_T/\sqrt{\theta}$ of 800, 900, 1000, and 1120 feet per second for each configuration. A range of weight flows was investigated at each speed from a high flow limit at which a pressure rise was no longer obtained at the tip to a flow at which blade tip stall occurred. An inlet pressure of 25 inches of mercury absolute was used for all tests.

Calculation Procedure

The average total-pressure ratio for the rotor with guide vanes was based on a mass-weighted integrated average of the isentropic power input that reduces to the following equation:

$$\left(\frac{P_2}{P_0}\right)_{av} = \left\{ \frac{\int_{r_{H,2}}^{r_{T,2}} \left[\left(\frac{P_2}{P_0}\right)^{\frac{\gamma-1}{\gamma}} - 1 \right] \rho_2 V_{x,2} r_2 \, dr}{\int_{r_{H,2}}^{r_{T,2}} \rho_2 V_{x,2} r_2 \, dr} + 1 \right\}^{\frac{\gamma}{\gamma-1}} \qquad (2)$$

The average adiabatic temperature-rise efficiency was calculated as a ratio of mass-weighted average isentropic power input to mass-weighted average total-temperature rise across the rotor as follows:

$$\eta_{ad} = \frac{\int_{r_{H,2}}^{r_{T,2}} T_0 \left[\left(\frac{P_2}{P_0} \right)^{\frac{\gamma-1}{\gamma}} - 1 \right] \rho_2 V_{x,2} r_2 \, dr}{\int_{r_{H,2}}^{r_{T,2}} (T_2 - T_0) \rho_2 V_{x,2} r_2 \, dr} \tag{3}$$

A numerical-average pressure ratio and adiabatic efficiency were used in evaluating the performance of the rotor without guide vanes, because preliminary calculations indicated that the difference between mass-flow average and numerical average was negligible for this configuration.

The average momentum efficiency was calculated as a ratio of the mass-weighted isentropic power input to mass-weighted momentum change across the rotor as follows:

$$\eta_M = \frac{\int_{r_{H,2}}^{r_{T,2}} T_0 \left[\left(\frac{P_2}{P_0} \right)^{\frac{\gamma-1}{\gamma}} - 1 \right] \rho_2 V_{x,2} r_2 \, dr}{\frac{1}{gJc_p} \int_{r_{H,2}}^{r_{T,2}} (U_2 V_{\theta,2} - U_1 V_{\theta,1}) \rho_2 V_{x,2} r_2 \, dr} \tag{4}$$

All other performance parameters used in this report were calculated directly from the measured pressure, temperature, and flow-angle data at stations 0, 1, and 2, respectively. Calculations across the rotor were made along assumed streamlines. The passage at stations 1 and 2 was divided into five equal radial increments, and the blade elements were rated with the streamlines assumed to be straight lines connecting these points, as is indicated in figure 4. This assumption was made to expedite the calculation procedure. The correct method for choosing streamlines would, of course, be to divide the passage into equal increments of mass flow. If this method were used, it would have been necessary to recalculate the streamlines at every data point, and thus also change the blade element rated at each operating point. Since this type calculation is very laborious, the same blade element was rated at all operating conditions.

[redacted]

Reliability of Data

In an investigation of this type, it is desirable to know the accuracy of measurement of the experimental data. It is not easy to determine the accuracy of each measurement quantitatively. The effects of radial and pulsating flows in addition to the circumferential variations were not evaluated completely from the instrumentation that was employed in this investigation. However, checks were made on the over-all performance data to estimate qualitatively the over-all accuracy of measurement.

Over-all performance. - Three weight-flow measurements were compared. One was calculated from the pressure and temperature measurements at the orifice plate, and the others were computed from an integration of the survey data at stations 1 and 2. The accuracy of the integrated weight flow is primarily dependent upon measurements of static pressure, total pressure, and flow angle, if the proper effective flow area is chosen, because temperature errors exert only a small influence on these calculations. Therefore, if the integrated and orifice weight flows agree, the static-pressure, total-pressure, and flow-angle measurements are probably correct. In this investigation, the discrepancy between the weight-flow measurements was never greater than 5 percent, and in most cases was less than 5 percent. The differences, in addition to instrument error, can be attributed to such things as the effects of wall boundary layer, blade wake, and instrument blockage in reducing the effective flow area from the geometrical area, as well as to the circumferential variations in flow that existed.

In addition to the weight-flow calculations, the efficiency of the compressor was calculated by two different methods from equations (3) and (4). These efficiencies are compared in figure 6. In calculating momentum efficiency (eq. (4)), the actual work done is based on the change in momentum through the rotor rather than on the temperature rise. An inherent error in the momentum-work-input concept associated with casing torque and element heat-transfer effects, which has been described in reference 7, results in values of efficiency higher than those calculated from equation (3). Therefore, the momentum efficiency was only utilized as a guide, and values of temperature-rise efficiency were used in plotting all curves and in making all computations. Figure 6 indicates that the discrepancy between the momentum and temperature-rise efficiencies was greater in the rotor with guide vanes than without. In the case of the rotor with guide vanes, the inlet whirl velocity as well as the outlet whirl had to be evaluated. Measurement of the inlet whirl could have introduced an additional source of error into the momentum-efficiency calculation that was not present in the rotor alone, because the inlet whirl velocity was zero in this case. The previous discussion is concerned with the over-all accuracy of measurement.

Blade-element performance. - The accuracy of measurement at each blade element is more difficult to determine than is the accuracy of the over-all data. No reliable check can be made on each individual measurement; therefore, the absolute values are subject to some question. However, it is believed that if reasonably good accuracy is obtained in the over-all results, the blade-element results will be reliable, in that the shape of the performance curves and a comparison of the relative measured values are valid.

In some cases the measured blade-element efficiency at the hub of the compressor exceeded 100 percent. This is probably due largely to the radial displacement of the low-energy air at the hub towards the tip. Reference 8, which is a study of the secondary-flow phenomena in a set of turbine nozzles, shows that it is possible for a loss that originates near the tip of the blade to be measured at the hub. In the case of a rotating blade row, the reverse would probably be true; that is, a loss that originates near the hub could be measured at the blade tip. If nearly complete centrifuging of the losses occurs toward the blade tip at station 2, the hub-station efficiency (based on a pressure ratio, P_2/P_0) will be very close to 100 percent (as was the case in the rotor with guide vanes). If the hub-station efficiency is then recomputed, based on P_2/P_1 (which is greater than P_2/P_0), the values could conceivably exceed 100 percent. Unfortunately, it was not possible to determine quantitatively the extent of the centrifuging of the losses in this investigation. It is entirely possible that measured values of temperature could also have affected the efficiency adversely.

Concluding remarks. - A satisfactory correlation of data was obtained between the two investigations, and the efficiency level of this unit was approximately the same as the full-stage investigation reported in reference 2. Therefore, the data were considered to be sufficiently accurate for reasonable correlation.

RESULTS AND DISCUSSION

Over-All Performance

Rotor with guide vanes. - The mass-averaged over-all performance is presented in figure 7. At design speed ($U_T/\sqrt{\theta}$ = 1120 ft/sec), a peak pressure ratio of 1.277 was reached at an efficiency of 0.85 and an equivalent weight flow of 23.75 pounds per second. A maximum efficiency at design speed of 0.905 was obtained at a weight flow of 28.18 and a pressure ratio of 1.186. Over the range of speeds investigated, the peak efficiency at each speed varied from 0.885 to 0.910. At speeds of 900, 1000, and 1120 feet per second, low-flow test points were not obtained because of a blade failure that occurred during operation in the stall region.

Rotor alone. - The over-all performance of the rotor in operation without inlet guide vanes is presented in figure 8. A tip speed of 1000 feet per second appears to be the best operating speed for this configuration, because relatively high pressure ratio can be obtained at good efficiency. At higher speeds, a rapid drop in efficiency occurs; at lower speeds, the pressure ratio is lower. Therefore, this speed will be considered to be design speed for this investigation. At an equivalent tip speed of 1000 feet per second, a peak pressure ratio of 1.297 was reached at an equivalent weight flow of 32.30 pounds per second and an efficiency of 0.89. A peak efficiency of 0.895 was reached at an equivalent weight flow of 33.60 pounds per second and a pressure ratio of 1.276. The weight flow for peak efficiency is very near the weight flow for peak pressure ratio. The drop in peak efficiency that occurs as the speed is increased from $U_T/\sqrt{\theta} = 1000$ to $U_T/\sqrt{\theta} = 1120$ is due primarily to a Mach number effect. This point will manifest itself in a later discussion.

Comparison. - The following table summarizes the design-speed over-all performance of both investigations:

Performance point	Rotor with guide vanes ($U_T/\sqrt{\theta}$ = 1120 ft/sec)			Rotor alone ($U_T/\sqrt{\theta}$ = 1000 ft/sec)		
	Total-pressure ratio, P_2/P_0	Adiabatic efficiency, η_{ad}	Equivalent weight flow, $\frac{W\sqrt{\theta}}{\delta}$, lb/sec	Total-pressure ratio, P_2/P_0	Adiabatic efficiency, η_{ad}	Equivalent weight flow, $\frac{W\sqrt{\theta}}{\delta}$, lb/sec
Peak pressure ratio	1.277	0.85	23.75	1.297	0.89	32.30
Peak efficiency	1.186	.905	28.18	1.276	.895	33.60

In addition to the design-speed summary presented in the table, it is desirable to compare the over-all performance at each tip speed (figs. 7 and 8) in order to obtain a better insight into the over-all performance characteristics of the rotor in operation with and without guide vanes. The values of peak efficiency were approximately the same except at a speed of 1120 feet per second, where the efficiency of the rotor alone dropped approximately 7 percent. By a comparison of the peak isentropic power input per pound of fluid at each speed T_1Y (or Y, since inlet total temperature was constant at all speeds), it was found that the isentropic power input was approximately 30 percent higher when the rotor was operating without inlet guide vanes. The peak pressure ratio for the rotor alone increased from approximately 1 percent at $U_T/\sqrt{\theta}$ = 800 feet per second to 8 percent at $U_T/\sqrt{\theta}$ = 1120 feet per second. The total energy addition per pound of fluid can be written as

$$H_2 - H_1 = U_2V_{\theta,2} - U_1V_{\theta,1} = c_p(T_2 - T_1) \tag{5}$$

From the definition of adiabatic efficiency:

$$\eta_{ad} = \frac{\frac{H_{2,i}}{H_1} - 1}{\frac{H_2}{H_1} - 1} = \frac{\left(\frac{P_2}{P_1}\right)^{\frac{\gamma-1}{\gamma}} - 1}{\frac{T_2}{T_1} - 1} \tag{6}$$

Combining equations (5) and (6) and solving for the pressure ratio result in:

$$\frac{P_2}{P_1} = \left[1 + \frac{\eta_{ad}\,(U_2V_{\theta,2} - U_1V_{\theta,1})}{c_pT_1}\right]^{\frac{\gamma}{\gamma-1}} \tag{7}$$

At constant wheel speed, inlet temperature, and efficiency, equation (7) indicates that the total-pressure ratio is dependent only upon the change in tangential velocity, $V_{\theta,2} - V_{\theta,1}$. Therefore, the change in tangential velocity must have been larger in the rotor alone. This may be more clearly illustrated by observing figure 1, which is a typical velocity diagram for the rotor with guide vanes. The value of y in this figure is indicative of the change in tangential velocity. Consider a typical velocity diagram for the rotor alone with the same rotational speed and the same relative inlet flow angle β_1', and therefore the same relative outlet flow angle β_2'. In this case (since β_1 is equal to zero), the value of axial velocity must increase to preserve the same inlet and outlet angles. This increase effectively increases the magnitude of the velocity components in the velocity diagram, including the value of y. Therefore, the pressure ratio is higher in the rotor alone.

The maximum equivalent weight flow increased approximately 21 percent at a tip speed of 1120 feet per second when the guide vanes were removed. At a tip speed of 800 feet per second, the increase amounted to 38 percent. These increases were expected. The addition of guide vanes to any annulus introduces new flow boundaries, and, therefore, instead of being a function of the axial component of velocity, the choking flow limit is a function of the absolute component at the guide-vane exit. The flow area will be effectively reduced as a direct function of the cosine of the guide-vane turning angle. It is, therefore, desirable to keep the guide-vane turning angle as low as possible for a high-mass-flow compressor design.

Blade-Element Performance

The procedure followed in the design of this axial-flow compressor consisted of two phases. Initially, it was necessary to select desirable velocity distributions at each radius of the compressor. Finally, the proper blade sections were chosen at each radial position and stacked in proper relation to each other to establish the design velocity distributions at each radius. The following three sections of the report are concerned with both phases of the design. The performance of each radial blade element is presented in a manner primarily for convenient use in selecting compressor blading, as well as for comparing calculated design velocity diagrams and measured values of velocity. Two independent variables are utilized as parameters for presenting the performance data in curve form, angle of incidence and equivalent weight flow. The use of equivalent weight flow as a plotting parameter is particularly desirable for a comparison of experimental results and calculated design conditions. It is usually convenient to compare various variables such as pressure ratio and efficiency at design weight flow. This procedure is followed in the report.

It is also advantageous to use incidence angle as an independent variable, since the range of angle of incidence, unlike range of equivalent weight flow, remains relatively constant at all speeds. Therefore, it is possible to relate the data at all blade speeds on a curve with only one basic parameter. Incidence angle is also frequently used as an independent variable in two-dimensional cascade plots. Therefore, its utilization provides a means of making a direct comparison of two-dimensional and three-dimensional (compressor) cascade plots. In addition, curves of angle of incidence against equivalent weight flow are also provided, so that a conversion from one parameter to the other can be made readily.

Performance of Rotor With Guide Vanes

A plot of local efficiency against equivalent weight flow at five radial positions along the blade height is shown in figure 9. The efficiency is computed from the pressure ratio between the depression tank and station 2; therefore, it provides an indication of the efficiency of the rotor and guide-vane combination. At all speeds investigated, the values of peak efficiency for radial positions B, C, D, and E exceeded 0.90. In contrast, however, the efficiency near the compressor tip (radial position A) usually was below 0.80. In order to analyze this problem (low tip efficiency) more completely, it is necessary to isolate the guide-vane losses and the rotor losses.

Guide-vane effects. Curves of guide-vane turning angle and guide-vane total-pressure-loss parameter plotted against radius ratio are

shown in figure 10 at design mass flow. Both the turning angle and loss parameter remained relatively constant as the mass flow varied. The design guide-vane turning-angle variation is also indicated. In general, the experimental data check the design very well over most of the flow passage (within 1°); however, at the hub and tip regions of the blade, the deviation is greater. This variation was probably caused by improper allowance for the boundary-layer and secondary-flow effects described in reference 5. The guide-vane total-pressure-loss parameter was determined from an area average of the preliminary circumferential surveys of pressure. The guide-vane loss remained relatively constant over the blade span except near the tip of the blade, where a sudden increase in loss was observed. Inasmuch as all radial measuring stations were not in the wall boundary-layer region, the boundary-layer effects on the loss were considered to be negligible. Therefore, this plot indicates that a portion of the compressor tip losses are caused by a thickening of the guide-vane wakes, which tended to substantially reduce the average total pressure at station 1.

Rotor performance. - The blade-element performance of the rotor (operating in conjunction with the inlet guide vanes) is presented at four tip speeds in figure 11. Curves of blade-element adiabatic efficiency (based on P_2/P_1), total-pressure ratio, angle of incidence, and relative inlet Mach number are plotted against equivalent weight flow. When these figures are compared with figure 9, a difference in rotor-tip peak efficiency of approximately 0.06 to 0.08 is obtained. Since the same values of total pressure were used at station 2 in the computation of the efficiency curves (figs. 9 and 11), indications are that a considerable portion of the tip element losses are caused by increased wake size near the guide-vane tip (radial position A, station 1).

In figure 12, curves of rotor total-pressure-loss parameter, relative inlet Mach number, and rotor turning angle are plotted against angle of incidence at four tip speeds for the five radial positions from hub to tip. At all radial positions except the tip, it is possible to operate over a fairly wide range of incidence angle without incurring serious total-pressure losses. At the hub section (fig. 12(e)), the losses are zero over most of the incidence-angle range. Reference 1, in which two-dimensional-cascade test results are obtained on a circular-arc airfoil of approximately the same camber and solidity, indicates a higher loss level. It was, therefore, believed that the low loss level at the hub that was obtained in this investigation was due to a radial shift of the low-energy air toward the tip section in addition to instrument errors described previously. If the optimum incidence angle is considered to be at the center of the low-loss incidence range, the optimum incidence angle in this investigation varied from -1° to 5° from tip to hub. Since the Mach number varies only slightly with incidence angle at each speed, these curves may be considered as loss curves at

constant Mach number. The difference in the loss curves (which is, in general, fairly small) at each speed can be attributed to the difference in Mach number at each speed. There appeared to be no Mach number effect on the turning-angle curves within the range of experimental accuracy, because all speeds plotted on a single curve.

Comparison with design. - In figure 12, in addition to the experimental turning-angle plots, the design turning-angle curves calculated from equation (1) are plotted as dotted lines. At the design incidence angle (2°), which is the incidence angle where the rule was applied, there is good agreement of the design rule and experimental results, except near the hub. At radial position E (fig. 12(e)), the data fall below the design line. The reason for this fact cannot be satisfactorily explained at this time.

Figure 13 is a plot of dimensionless energy addition against radius ratio at design speed. This curve indicates that at the design weight flow the design energy addition was not attained. The design assumption of efficiency (0.90) proved to be very accurate at design weight flow (fig. 7). Therefore, the effects of efficiency on design energy addition were eliminated. Achieving design-point operation was of secondary importance in this investigation; therefore, no passage-area allowance for boundary was made. Because of the boundary-layer buildup at stations 1 and 2, the axial velocity at design weight flow at station 1 was higher than design. The ratio of the measured mean axial velocity to the design axial velocity $V_{x,m}/V_{x,d}$ was 1.05. At station 2 a further increase in axial velocity resulted ($V_{x,m}/V_{x,d} = 1.09$). Since the axial velocity was high at station 1, design angle of incidence was not attained at design weight flow, as is indicated by figure 11(a). A low angle of incidence and an acceleration of axial velocity through the rotor both contributed to reducing the energy addition below the design value. Since the design energy addition was low, it was expected that the pressure ratio (fig. 7) would fall below the design value.

Radial equilibrium. - Curves of dimensionless axial velocity against radius ratio at design speed at stations 1 and 2 are given in figure 14. Plots corresponding to three different values of weight flow are shown in each figure, high flow, low flow, and maximum efficiency. The dotted curves are distributions of dimensionless axial velocity calculated by integrating equation (14) of reference 9. The equation is as follows:

$$\frac{\partial H}{\partial r} = F_r + T\frac{\partial s}{\partial r} + \frac{V_\theta}{r}\frac{\partial (rV_\theta)}{\partial r} + V_x\frac{\partial V_x}{\partial r} - V_x\frac{\partial V_r}{\partial_x} \qquad (8)$$

The integration of this equation was based on the following assumptions:

1. Since the calculations were made before and after each blade row, the radial force exerted on the gas by the blades was zero ($F_r = 0$).

2. Radial accelerations of velocity were assumed to be equal to zero; therefore, $V_x \frac{\partial V_r}{\partial x} = 0$.

3. The variation in entropy along the radius was assumed to be zero; therefore, $T \frac{\partial s}{\partial r} = 0$.

Equation (8) then reduced to

$$\frac{\partial H}{\partial r} = \frac{V_\theta}{r} \frac{\partial (rV_\theta)}{\partial r} + V_x \frac{\partial V_x}{\partial r} \tag{9}$$

Figures 14(a) and (b) indicate that the design assumption of simple radial equilibrium was reasonably accurate both before and after the rotor. In order to find the effect of the variation in entropy along the radius after the rotor on equation (9), the term $T \frac{\partial s}{\partial r}$ was expressed in terms of measured pressures and temperatures and added to equation (9). The results of this calculation are indicated in figure 14(c), which shows that the computed axial velocity will more closely approximate measured values if the entropy-gradient term is included in the equilibrium calculation.

Rotor-outlet conditions. - In figure 15, the rotor-outlet absolute air angle and rotor-outlet absolute Mach number are plotted against radius ratio at the maximum efficiency point at design speed. This curve represents the stator-inlet conditions and is presented to show the range of inlet conditions which would be encountered in the stator-design problem.

Performance of Rotor Alone

Blade-element performance. - The blade-element performance of the rotor without inlet guide vanes is presented at four tip speeds in figure 16. Curves of blade-element adiabatic efficiency, total-pressure ratio, angle of incidence, and relative inlet Mach number are plotted against equivalent weight flow. In figure 17, curves of total-pressure-loss parameter, relative inlet Mach number, and rotor turning angle are plotted against angle of incidence at four tip speeds for the five radial positions. The optimum incidence angle varies from approximately

1° at the tip (radial position A, fig. 17(a)) to approximately 5° at radial position D (fig. 17(d)). At the hub (fig. 17(e)), because of the shape of the loss curves, the optimum incidence angle could not be determined. Figure 17 indicates that there is an appreciable variation of Mach number with incidence angle. This tends to reduce the slope of the loss curves somewhat at the high incidence angles. At radial positions B, C, and D (figs. 17(b) to (d)) a slight dip in the turning-angle curves was noted. The reason for this dip cannot be explained definitely; however, it is possible that a slight flow separation and reattachment could have occurred in the region of the dip. Again, within the range of experimental accuracy, there appeared to be no effect of Mach number on the turning-angle curves. The dashed curves indicate the design rule. At the design angle of incidence (2°), the data at radial positions A, B, and C agree with the rule of reference 6 reasonably well (within 1.5°). At radial positions D and E, data points at design incidence were not obtained because of the large gradient of incidence angle imposed by removal of the guide vanes. Therefore, a check with the design rule could be made only by extrapolation of the turning-angle curve to design incidence. Since there was some scatter of data in the end regions of the turning-angle curves at radial positions D and E, accurate extrapolation proved to be difficult. Therefore, the check on the design rule at these radial positions was not considered accurate enough to warrant discussion.

Radial equilibrium. - Curves of dimensionless axial velocity against radius ratio at station 2 at a tip speed of 1000 feet per second are shown in figure 18. Three plots, corresponding to three different values of weight flow, are shown, high flow, low flow, and maximum efficiency. In figure 18(a), the dashed curves represent the distributions of dimensionless axial velocity that were calculated by means of equation (9). The dashed curves in figure 18(b) have also been calculated from equation (9), with the entropy-gradient term included in the calculation. The results, similar to those for the rotor with guide vanes, indicate that a better correlation of calculated curves and experimental data is obtained if the entropy-gradient term is included in the equation for radial equilibrium.

Rotor-outlet conditions. - Figure 19, which is similar to figure 15 and presents the rotor-outlet absolute air angle and rotor-outlet Mach number against radius ratio at the maximum-efficiency point at a tip speed of 1000 feet per second, represents the stator-inlet conditions that would probably be used for a stator-blade design.

Comparison of Rotor Investigations

In order to integrate the previous discussions of the blade-element parameters used in evaluating the performance of both configurations, it

was desirable to compare the performance curves. By means of this comparison, the regions of agreement and disagreement of the performance parameters would be manifest.

Blade-element performance. When figure 11 is compared with figure 16, several differences in performance are observed. The blade-element peak efficiencies covered the same range of values except at a tip speed of 1120 feet per second. The pressure-ratio level and the Mach number at each radial position at each speed were higher for the rotor with no guide vanes, because velocity diagrams at each radial position were effectively scaled up. The reason for these facts was explained in detail in the section on Over-All Performance.

The rate of change of incidence angle with weight flow is greater for the rotor with guide vanes. Therefore, for a given increment of incidence angle, a greater increment of weight flow will be obtained for the rotor alone. The angle of incidence from hub to tip at each weight flow at each speed is relatively constant for the rotor with guide vanes. In contrast, this angle varies approximately 8° for the rotor alone. The incidence-angle variation, however, did not seem to cause any appreciable mismatching of the blade sections, as is indicated by the fact that the value of weight flow for peak efficiency at each radial position at each speed was relatively constant. This trend cannot be reconciled with the cascade data of reference 1. The results of reference 1 indicate that the hub section of the blade would be operating in the high-loss region at values of incidence angle incurred in the investigation of the rotor alone. Therefore, it appears that three-dimensional effects alleviated the problem of high hub incidence angles. It is possible that a radial shift of the low-energy air towards the tip resulted in a high indicated efficiency at the hub before separation, in spite of the very high incidence angles. In addition, because of the flow-area blockage caused by finite blade thickness, an acceleration of the flow ahead of the blades may have delayed flow separation associated with high incidence angles.

In a comparison of figure 12 with figure 17, differences in performance are also noted. In the previous discussions of these figures, it was stated that the optimum incidence-angle variation from hub to tip in the rotor with guide vanes is from -1° to 5°; in the rotor alone, the values of optimum incidence angle are slightly higher, ranging from 1° at the tip to 5° at radial position D (the hub optimum incidence angle could not be determined). The Mach number level is higher for the rotor alone, and it appears that values of optimum incidence increase as Mach number increases. This trend is also indicated by the cascade data of reference 1. In the regions where a comparison of the design turning-angle rule and the experimental data could be made, the results indicate that the design rule predicted accurately the turning angle except at radial position E, where a slight underturning was observed.

In addition, a comparison of the tip turning-angle curves (figs. 12(a) and 17(a)) indicates that a wider range of angle of incidence could be covered before tip stall with the rotor alone. The point at which tip stall occurs is assumed to be that value of incidence where the maximum turning angle occurred. Therefore, a wider weight-flow range could be covered before tip stall in the rotor alone for two reasons. The incidence-angle range before tip stall is greater, and, as previously indicated, the rate of change of incidence angle with weight flow is smaller for the rotor alone. Therefore, a greater weight-flow range is possible in the rotor alone.

Blade-loading and Mach number effects. - It has been generally established that one of the largest sources of losses in axial-flow compressors occurs when the flow separates from the suction surface of the blades. The flow separation arises from excessive suction-surface velocity gradients (high blade loading) and from the results of shocks and boundary-layer interactions that occur with high relative inlet Mach numbers. As reported in reference 10, blade loading can be adequately described by the diffusion factor, which can be written as

$$D = \left(1 - \frac{V_2'}{V_1'}\right) + \frac{V_{\theta,2} - V_{\theta,1}}{2\sigma V_1'} \qquad (10)$$

Values of diffusion factor have significance at or very near the optimum incidence angle of the blade. The first term is a function of the relative velocity ratio, and the second term is proportional to the blade lift coefficient. In reference 10, equation (10) was used to correlate data obtained from numerous single-stage-compressor test rigs on the basis of the total-pressure-loss parameter ω at or near optimum incidence angle at values of sub-limiting Mach numbers. The limiting Mach number is defined as the Mach number where losses begin to increase very rapidly.

In order to compare results of the two rotor investigations and to examine the differences in blade-loading and Mach number levels, the measured total-pressure-loss parameter is plotted in figure 20 against diffusion factor. The data points represent both investigations and are either at or near the optimum incidence angle, since values of diffusion factor apply only in this range.

At radial positions B, C, D, and E, only a relatively small range of diffusion factor was covered. In this range, the losses were of the same order of magnitude as those reported at the hub- and mean-radius positions in reference 10. This being the case, it was felt that flow separation did not occur near optimum incidence. At these radial positions, a good correlation of data was obtained for both rotor

investigations. Since the loss level was of the same order of magnitude in both cases, even though the Mach number level was different, these plots indicate that the relative inlet Mach number did not have any measurable effect on the performance in the range of Mach numbers experienced.

At radial position A, a much wider range of losses and diffusion factors was covered. As the diffusion factor increased, the loss increased. This type of loss variation with diffusion factor was also reported in reference 10, and is shown on the curve by the dashed lines. The measured diffusion factors are reasonably accurate, because it is believed that the measured velocities are correct, in view of the integrated weight-flow checks. Excluding the data for the rotor alone at $U_T/\sqrt{\theta}$ = 1120 feet per second, the data from both investigations appear to fall on a single curve that is somewhat higher than the range of values given in reference 10. The higher losses might be due to experimental inaccuracy and the transporting of low-energy air from the hub to the tip in the rotor, as mentioned previously. The only data that do not appear to agree with all the rest are the loss parameters at the two lower values of diffusion factor at $U_T/\sqrt{\theta}$ = 1120 feet per second for the rotor alone. These higher losses are an indication that the limiting relative Mach number for this blade section has been exceeded for these two points for this diffusion-factor range. The value for the limiting Mach number appears to be between 1.10 and 1.20 for the blade element near the tip, on the basis of this diffusion correlation. This value is considerably higher than that at which any conventional airfoil currently in use has been able to operate efficiently. The higher value is partly due to the fact that the circular-arc airfoil has a much thinner nose; therefore, for a given inlet Mach number, both the blade maximum surface velocity and the channel mean velocity will be lower than those of conventional airfoils. Since the channel mean velocity determines the "choke point", higher inlet Mach numbers may be tolerated before the shock and boundary-layer losses associated with choking flow are incurred.

If the data points at $U_T/\sqrt{\theta}$ = 1120 feet per second for the rotor alone are again not considered in figure 20(a), the range of values of diffusion factor covered in both investigations is the same. Therefore, approximately the same loss-parameter level was obtained in both investigations, even though considerably higher pressure ratios were obtained for the rotor alone.

SUMMARY OF RESULTS

A 14-inch-diameter axial-flow-compressor rotor with a hub-tip diameter ratio of 0.50 was operated to investigate the blade-element

characteristics as well as the over-all performance of a set of circular-arc blades over a range of inlet relative Mach number from 0.40 to 0.82 with inlet guide vanes installed and from 0.44 to 1.22 with the guide vanes removed. The following results were obtained from this investigation:

1. At design blade tip speed of 1120 feet per second, a peak pressure ratio of 1.277 was reached at an efficiency of 0.85 and an equivalent weight flow of 23.75 pounds per second for the rotor with guide vanes. A maximum design-speed efficiency of 0.905 was obtained at a weight flow of 28.18 and a pressure ratio of 1.186.

2. At an equivalent tip speed of 1000 feet per second, which was considered to be the best operating speed for the rotor alone, a peak pressure ratio of 1.297 was reached at an equivalent weight flow of 32.30 pounds per second and an efficiency of 0.89. A peak efficiency of 0.895 was reached at an equivalent weight flow of 33.60 pounds per second and a pressure ratio of 1.276.

3. The over-all compressor tip efficiency was reduced 6 to 8 percent because of losses in the inlet guide vanes.

4. In both investigations, it was possible to operate over a wide range of incidence angle at all radial positions with no large losses except at the blade tip.

5. Over the range of Mach numbers investigated, no Mach number effect on the turning angle was detected.

6. At the design incidence angle, the design turning-angle rule predicted accurately the turning at all radial positions except the hub section. At the hub, slight underturning resulted.

7. The design assumption of simple radial equilibrium was relatively accurate, in that reasonably good checks of calculated and measured axial velocity were obtained. However, when the entropy-gradient term was included in the radial equilibrium equation, there was better agreement between the measured data and calculated values of axial velocity.

8. The optimum incidence angle appeared to increase as Mach number increased in this investigation.

9. In the investigation of the rotor alone at a tip speed of 1120 feet per second, there were indications that the limiting relative Mach number (which was determined to be between 1.10 and 1.20) had been exceeded. Therefore, the over-all peak efficiency was reduced approximately 7 percent.

Lewis Flight Propulsion Laboratory
National Advisory Committee for Aeronautics
Cleveland, Ohio

APPENDIX - SYMBOLS

The following symbols are used in this report:

A,B,C, D,E	blade measuring stations
c	blade chord, in.
c_p	specific heat at constant pressure, 0.241 Btu/(lb)(deg)
D	diffusion factor $\left(1 - \frac{V_2'}{V_1'}\right) + \frac{V_{\theta,2} - V_{\theta,1}}{2\sigma V_1'}$
F	force
g	acceleration due to gravity, 32.2 ft/sec^2
H	total enthalpy (actual work input per pound calculated from total-temperature rise), ft-lb/lb
h	dimensionless axial velocity, ratio of axial velocity to tip speed
i	angle of incidence, angle between tangent to blade mean camber line at leading edge and inlet-air direction, deg
J	mechanical equivalent of heat, 778 ft-lb/Btu
K	arbitrary constant
M	Mach number
m	coefficient - function of blade-setting angle (angle between chord and axis)
P	total pressure, lb/sq ft
p	static pressure, lb/sq ft
r	radius
S	blade spacing, in.
s	entropy, Btu/(lb)(deg)

[redacted]

T	temperature, $^{\circ}R$
t	blade thickness, (percent of chord length)
U	blade speed, ft/sec
V	velocity, ft/sec
W	weight flow, lb/sec
x	ratio of absolute tangential velocity to rotor tip speed
Y	$\left(\frac{P_2}{P_1}\right)^{\frac{\gamma-1}{\gamma}} - 1$
y	ratio of change in tangential velocity through rotor to rotor tip speed
z	radius ratio, r/r_T or blade-speed ratio U/U_T
β	angle between velocity vector and rotor axis, deg
γ	ratio of specific heats
Δ	deviation angle, angle between tangent to mean camber line at blade trailing edge and air direction
δ	ratio of inlet total pressure to standard NACA sea-level pressure, 2116.2 lb/sq ft
η_{ad}	adiabatic efficiency
η_M	momentum efficiency
θ	ratio of inlet total temperature to standard NACA sea-level temperature, 518.6° R
μ	blade-setting angle, angle between chord and axis, deg
ρ	air density, slugs/cu ft
σ	ratio of chord to spacing, c/S
φ	blade camber angle, deg

[redacted]

ω total-pressure-loss parameter, $\left(\frac{P_2' - P_1'}{P_1 - p_1}\right)$ or $\left(\frac{P_1 - P_0}{P_0 - p_{GV}}\right)$

Subscripts:

av	average
d	design condition
GV	guide-vane inlet
H	compressor hub
i	ideal condition
m	mean
P	pressure surface
r	radial direction
S	suction surface
T	compressor tip
x	axial direction
θ	tangential direction
0	depression-tank measuring station
1	measuring station after guide vanes
2	measuring station after rotor

Superscript:

'	relative to rotor

REFERENCES

1. Andrews, S. J.: Tests Related to the Effect of Profile Shape and Camber Line on Compressor Cascade Performance. Rep. No. R-60, British N.G.T.E., Oct. 1949.

2. Lieblein, Seymour, Lewis, George W., Jr., and Sandercock, Donald M.: Experimental Investigation of an Axial-Flow Compressor Inlet Stage Operating at Transonic Relative Inlet Mach Numbers. I - Over-All Performance of Stage with Transonic Rotor and Subsonic Stators Up to Rotor Relative Inlet Mach Number of 1.1. NACA RM E52A24, 1952.

3. Voit, Charles H., and Thomson, Arthur R.: An Analytical Investigation Using Aerodynamic Limitations of Several Designs of High Stage Pressure Ratio Multistage Compressors. NACA TN 2589, 1951.

4. Lieblein, Seymour: Turning-Angle Design Rules for Constant-Thickness Circular Arc Inlet Guide Vanes in Axial Annular Flow. NACA TN 2179, 1950.

5. Lieblein, Seymour, and Ackley, Richard H.: Secondary Flows in Annular Cascades and Effects on Flow in Inlet Guide Vanes. NACA RM E51G27, 1951.

6. Carter, A. D. S., and Hughes, Hazel P.: A Theoretical Investigation into the Effect of Profile Shape on the Performance of Airfoils in Cascade. R. & M. No. 2384, British A.R.C., Mar. 1946.

7. Goldstein, Arthur W., and Schacht, Ralph L.: Performance of a Swept Leading Edge Rotor of the Supersonic Type with Mixed Flow. NACA RM E52K03, 1953.

8. Rohlik, Harold E., Allen, Hubert W., and Herzig, Howard Z.: Study of Secondary-Flow Patterns in an Annular Cascade of Turbine Nozzle Blades with Vortex Design. NACA TN 2909, 1953.

9. Wu, Chung-Hua, and Wolfenstein, Lincoln: Application of Radial-Equilibrium Condition to Axial-Flow Compressor and Turbine Design. NACA Rep. 955, 1950. (Supersedes NACA TN 1795.)

10. Lieblein, Seymour, Schwenk, Francis C., and Broderick, Robert L.: Diffusion Factor for Estimating Losses and Limiting Blade Loadings in Axial-Flow-Compressor Blade Elements. NACA RM E53D01, 1953.

TABLE I. - GUIDE-VANE GEOMETRY

Radial position	Blade camber angle, φ, deg	Blade chord, c, in.	Chord-to-spacing ratio, σ
Hub	26.6	1.08	1.37
Mean	36.5	1.47	1.24
Tip	57.2	2.25	1.43

Compressor diam., in.	14
Compressor hub-tip diam. ratio	0.50
Blade radius of curvature, in.	2.346
Material	0.060-in. sheet steel
Blade leading- and trailing-edge radii, in.	0.030
Number of blades	28

TABLE II. - ROTOR BLADE DETAILS

Radial position	Blade camber angle, φ, deg	Blade thickness, t, percent chord	Chord-to-spacing ratio, σ	Suction-surface arc radius, in.	Pressure-surface arc radius, in.
Hub	31.2	10.0	1.57	1.74	7.97
Mean	16.1	7.5	1.05	2.79	214.88
Tip	0	5.0	.785	8.28	-8.28

NACA

Compressor diam., in.	14
Compressor hub-tip diam. ratio	0.50
Rotor blade chord, in.	1.50
Rotor blade leading-edge radius, in.	0.010
Rotor blade trailing-edge radius, in.	0.030
Number of blades	23

TABLE III. - INSTRUMENTATION SUMMARY

Station	Radial measuring position		Measurement	Instrument	Circumferential positions
	Station	Radius, ft			
Depression tank, 0			Total pressure	Wall taps	4
			Total temperature	Thermocouple probe	3
After guide vanes, 1	Tip	0.5833	Total pressure	Claw total-pressure probe	1
	A	.5529	Static pressure	Straight-support wedge-type static-pressure probe	1
	B	.4937		Wall taps	4
	C	.4346			
	D	.3754			
	E	.3162	Flow angle	Claw total-pressure probe	1
	Hub	.2867			
After rotor blades, 2	Tip	0.5833	Total pressure	Claw total-pressure probe	1
	A	.5562	Static pressure	"L"-support wedge-type static-pressure probe	1
	B	.5021		Wall taps	8
	C	.4479			
	D	.3937			
	E	.3396	Total temperature	5-Tip spike-type total-temperature rake	3
	Hub	.3125	Flow angle	Claw total-pressure probe	1

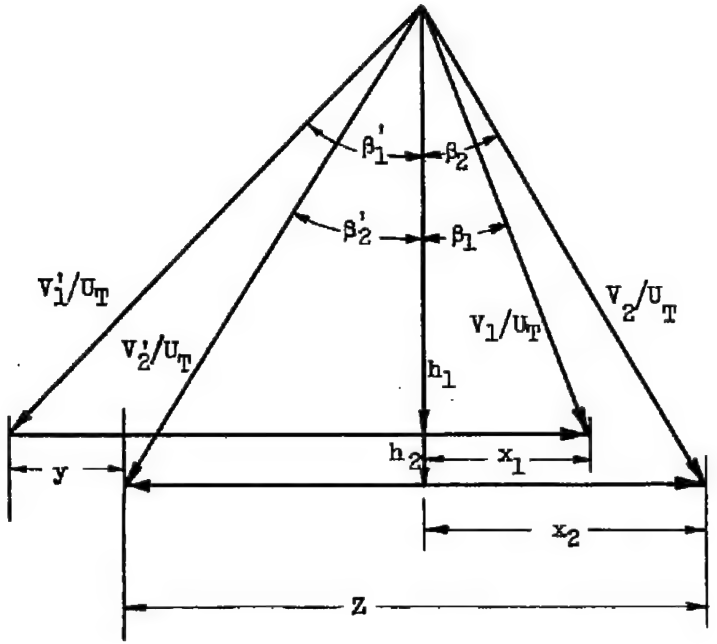

Radial position	U_T, ft/sec	V_1/U_T	V_2/U_T	V_1'/U_T	V_2'/U_T	h_1	h_2	z	x_1	x_2	y	β_1', deg	β_2', deg	β_1, deg	β_2, deg
Hub		0.5819	0.7522	0.6518	0.5932	0.5584	0.5921	0.5	0.1639	0.4639	0.300	31.0	3.5	16.4	38.1
Mean		0.5524	0.6659	0.7062	0.5806	0.4946	0.4946	0.75	0.2459	0.4459	0.200	45.5	31.6	26.4	42.0
Tip	1120	0.5080	0.5907	0.7762	0.6272	0.3881	0.3474	1.0	0.3278	0.4778	0.150	60.0	56.4	40.2	54.0

NACA

Figure 1. - Design velocity diagrams computed at standard conditions for rotor with guide vanes.

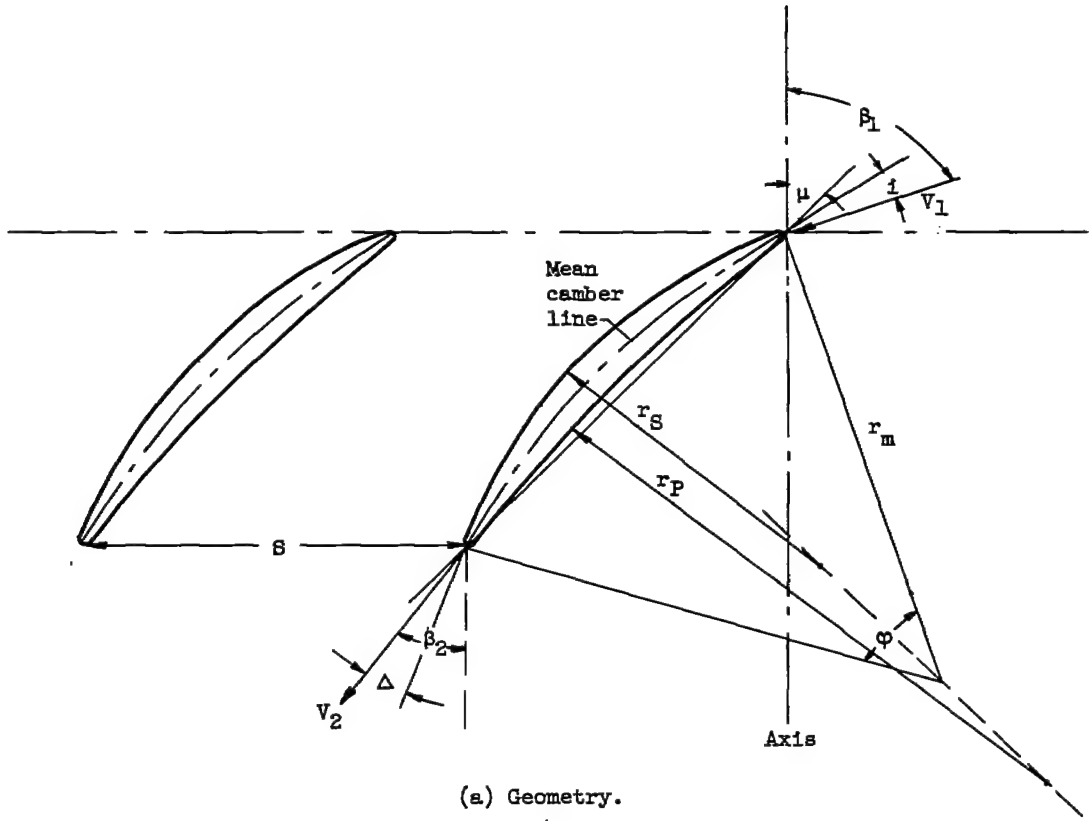

(a) Geometry.

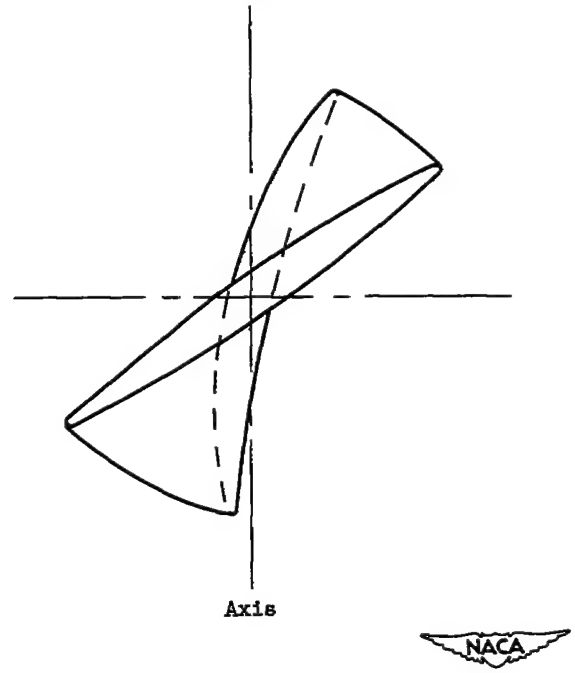

(b) Top view.

Figure 2. - Typical rotor blade section.

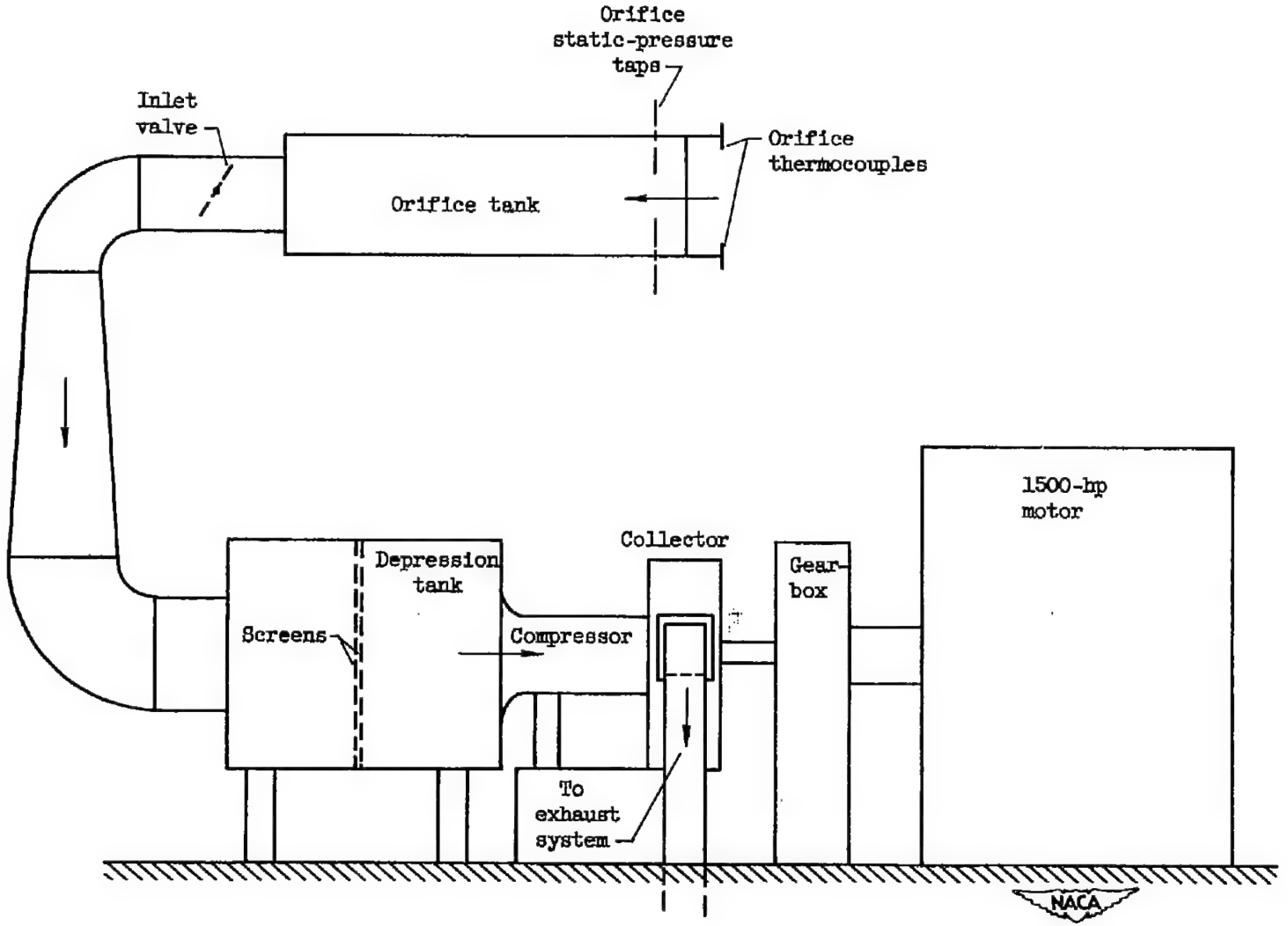

Figure 3. - Experimental setup.

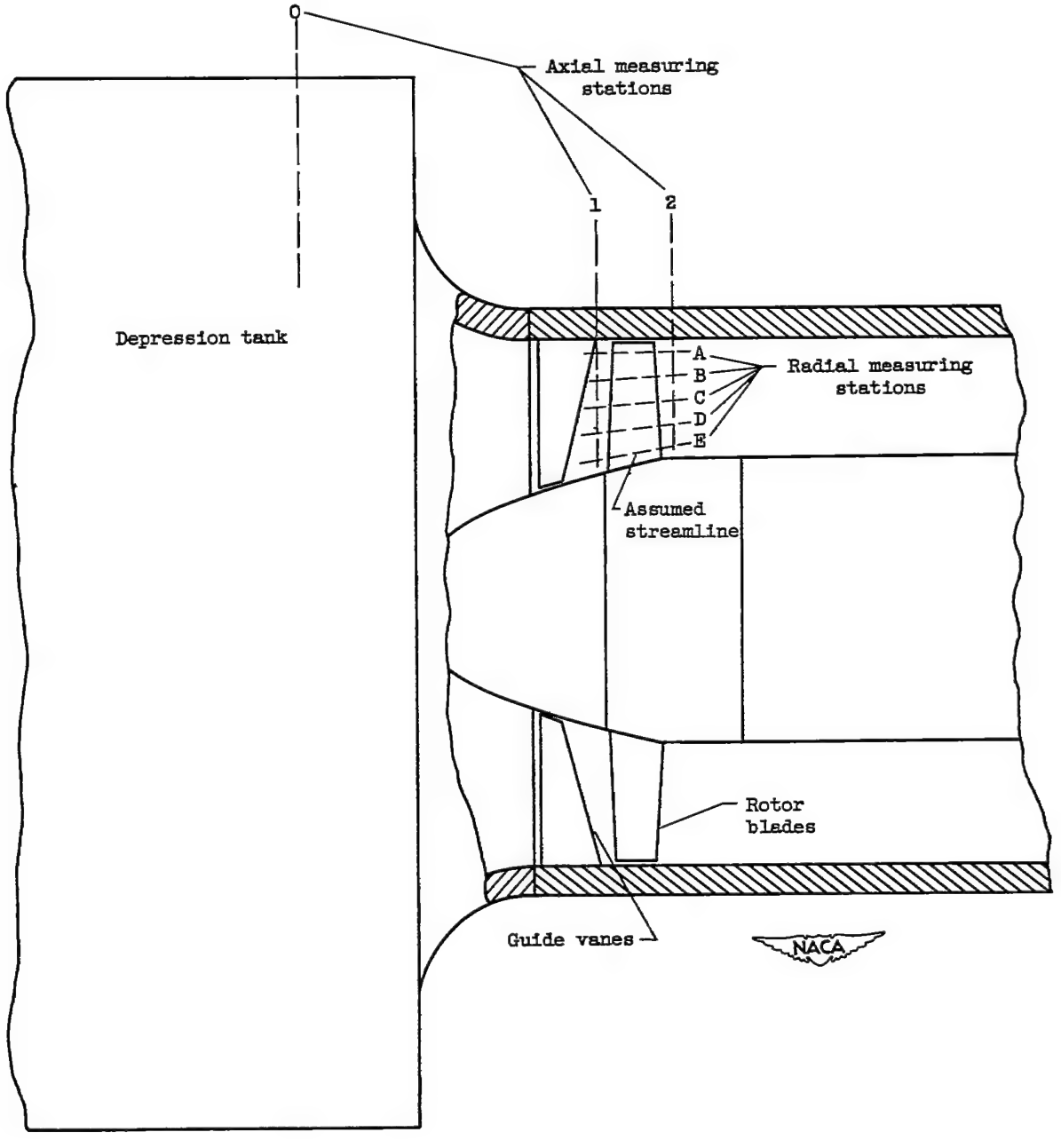

Figure 4. - Experimental compressor.

(a) Straight-support static-pressure wedge. Station 1.

(b) Spike-type thermocouple rake. Station 2.

(c) Claw total-pressure tube. Stations 1 and 2.

(d) "L"-support static-pressure wedge. Station 2.

Figure 5. - Types of instrumentation.

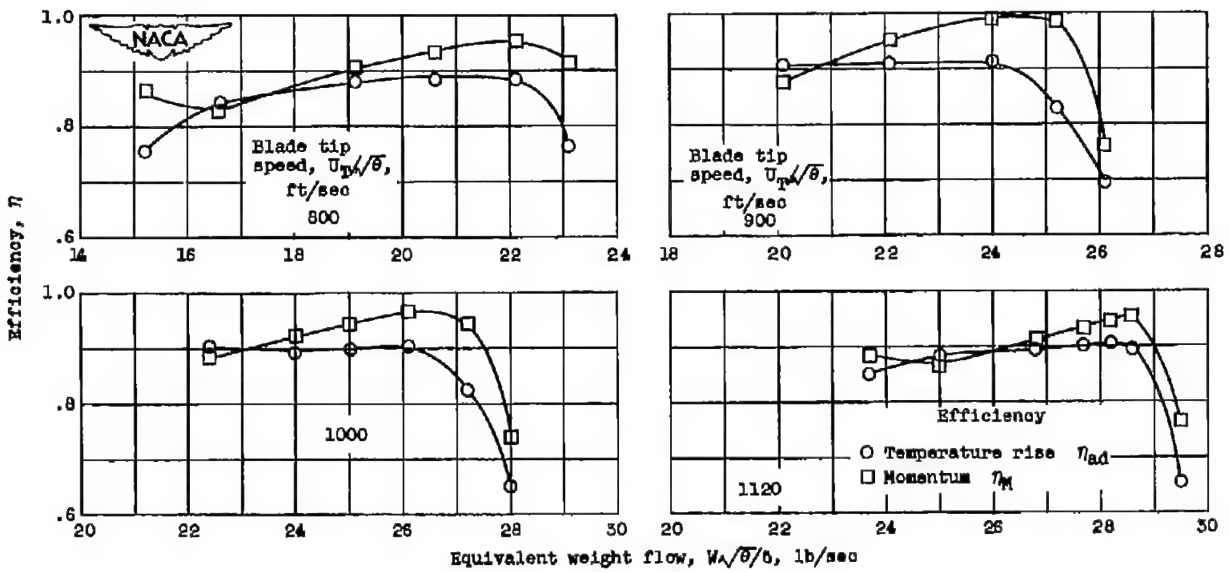

(a) Rotor with guide vanes.

Figure 8. - Comparison of temperature-rise and momentum efficiencies at four equivalent tip speeds.

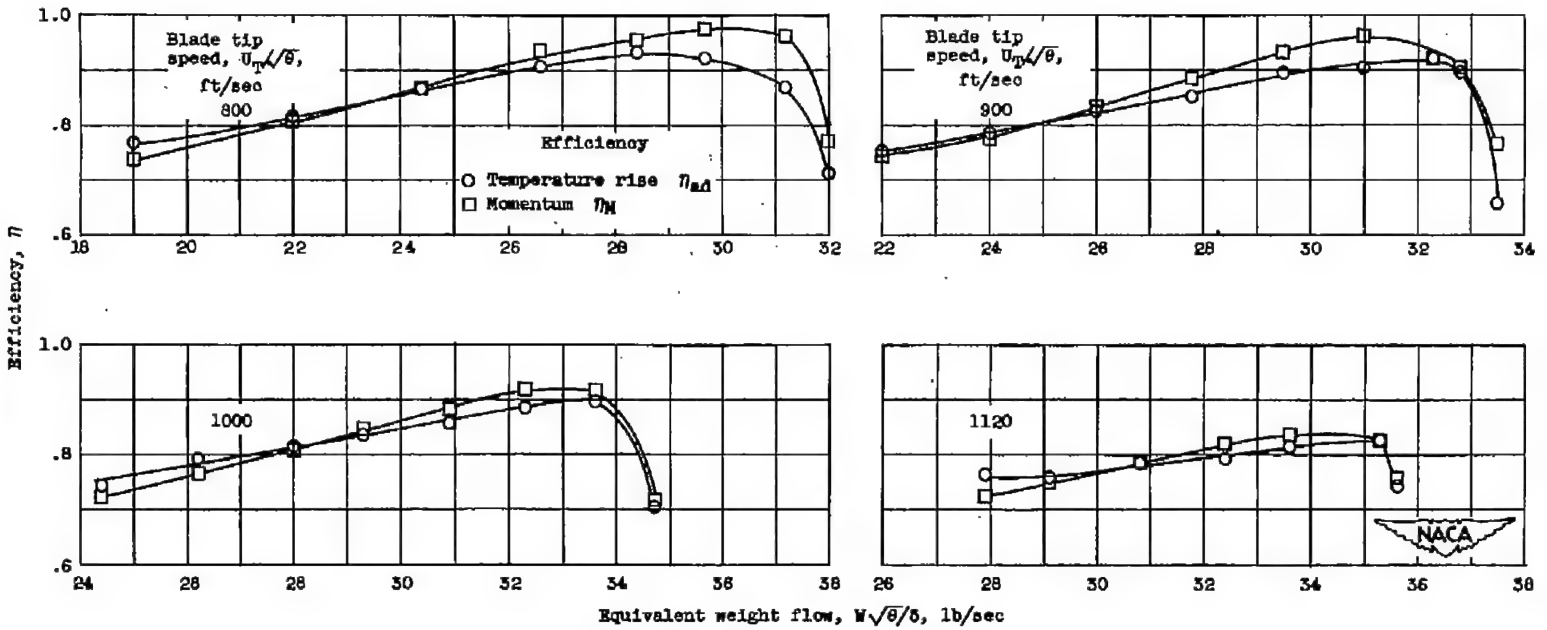

(b) Rotor alone.

Figure 6. - Concluded. Comparison of temperature-rise and momentum efficiencies at four equivalent tip speeds.

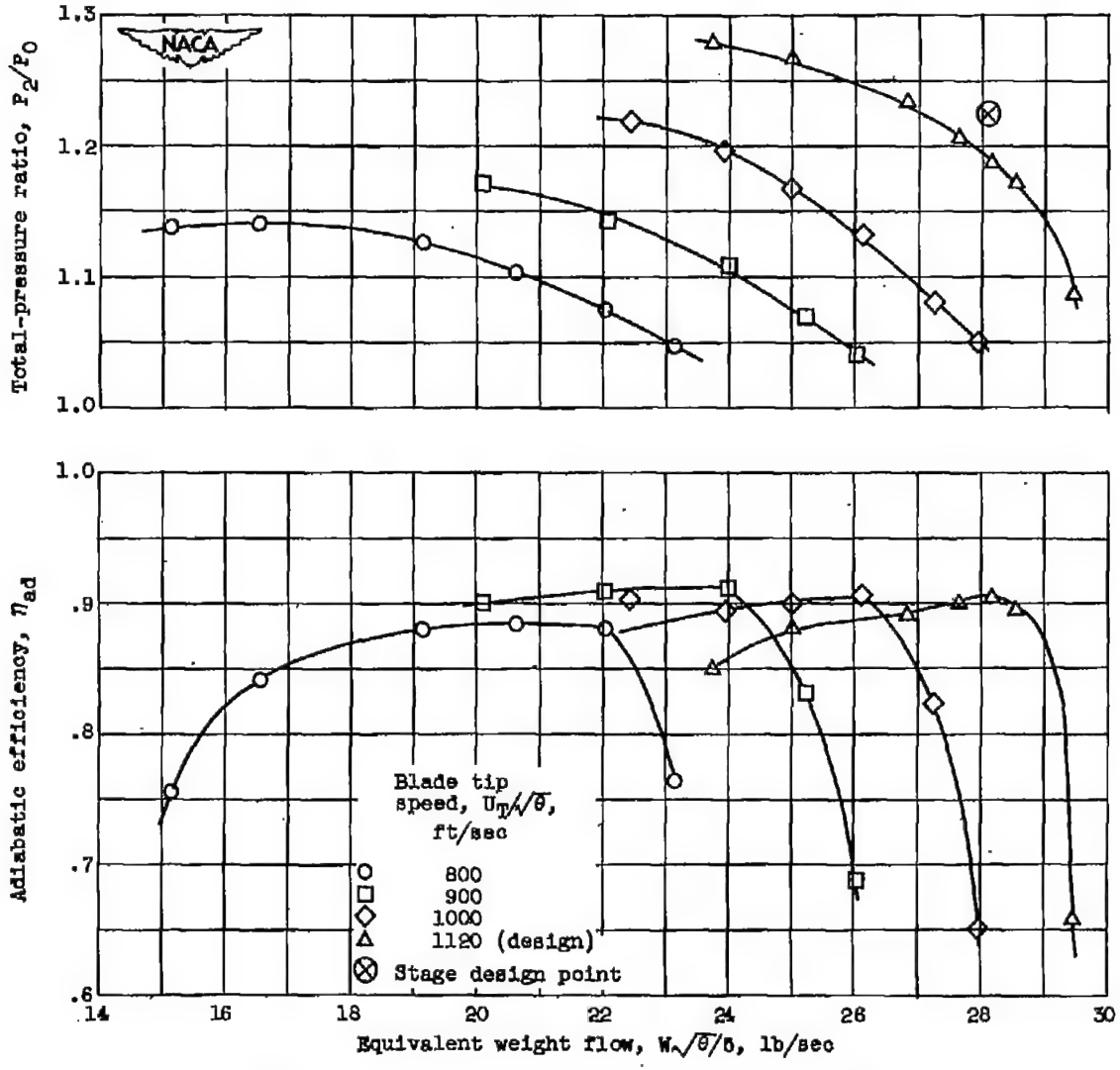

Figure 7. - Over-all performance of rotor with guide vanes.

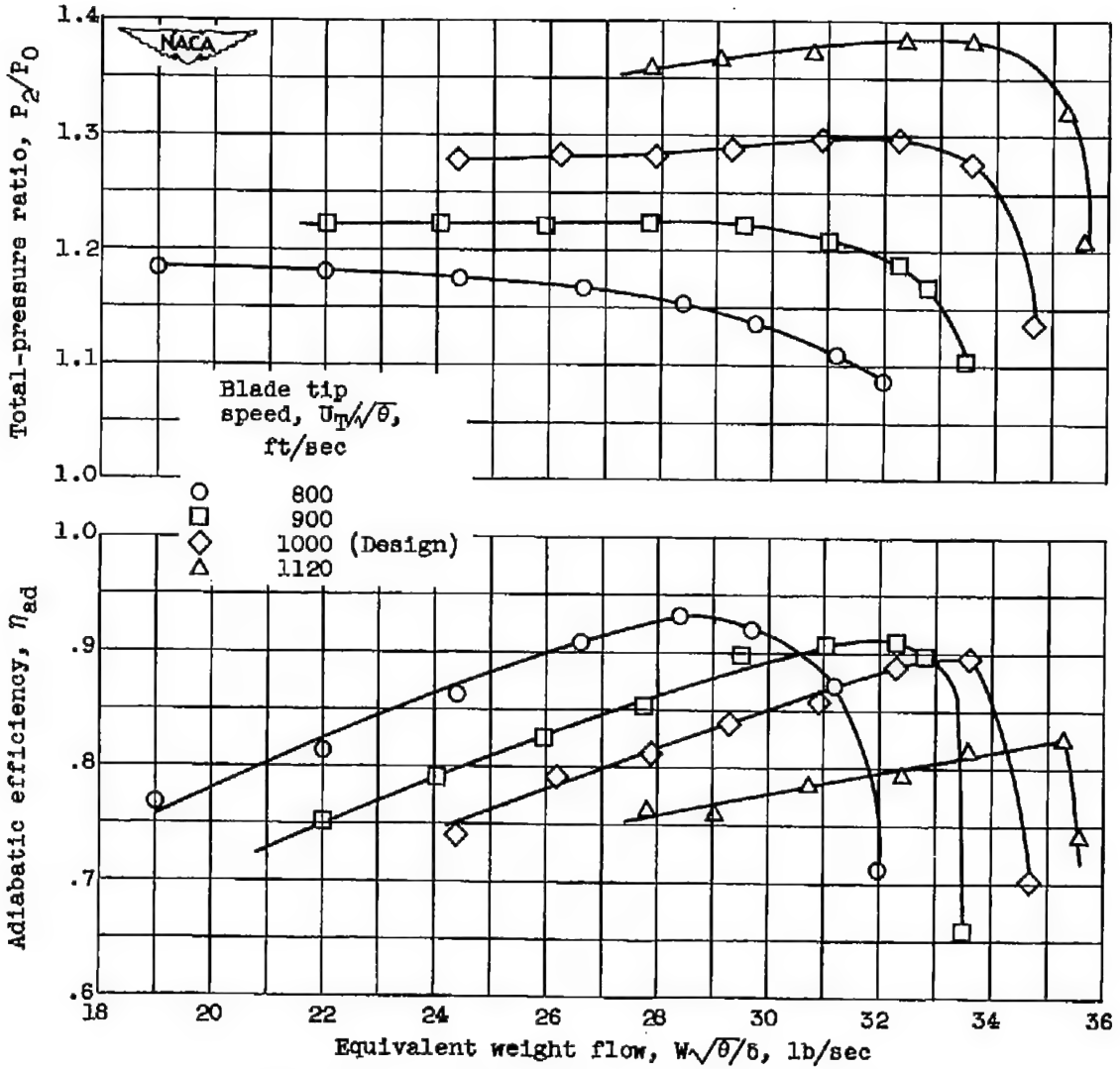

Figure 8. - Over-all performance of rotor alone.

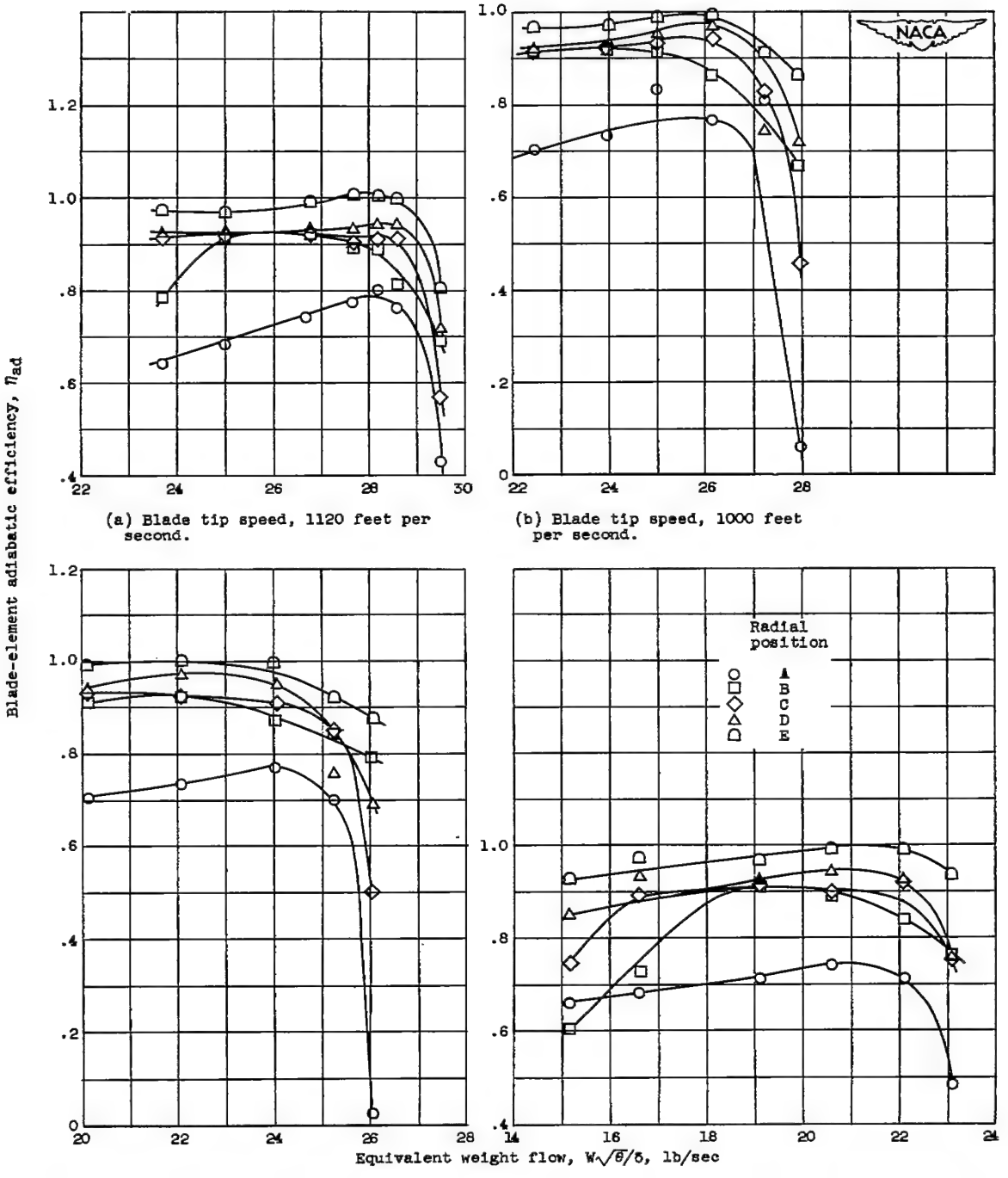

(a) Blade tip speed, 1120 feet per second.

(b) Blade tip speed, 1000 feet per second.

(c) Blade tip speed, 900 feet per second.

(d) Blade tip speed, 800 feet per second.

Figure 9. - Variation of blade-element efficiency (including guide-vane losses) with equivalent weight flow for rotor with guide vanes.

[redacted]

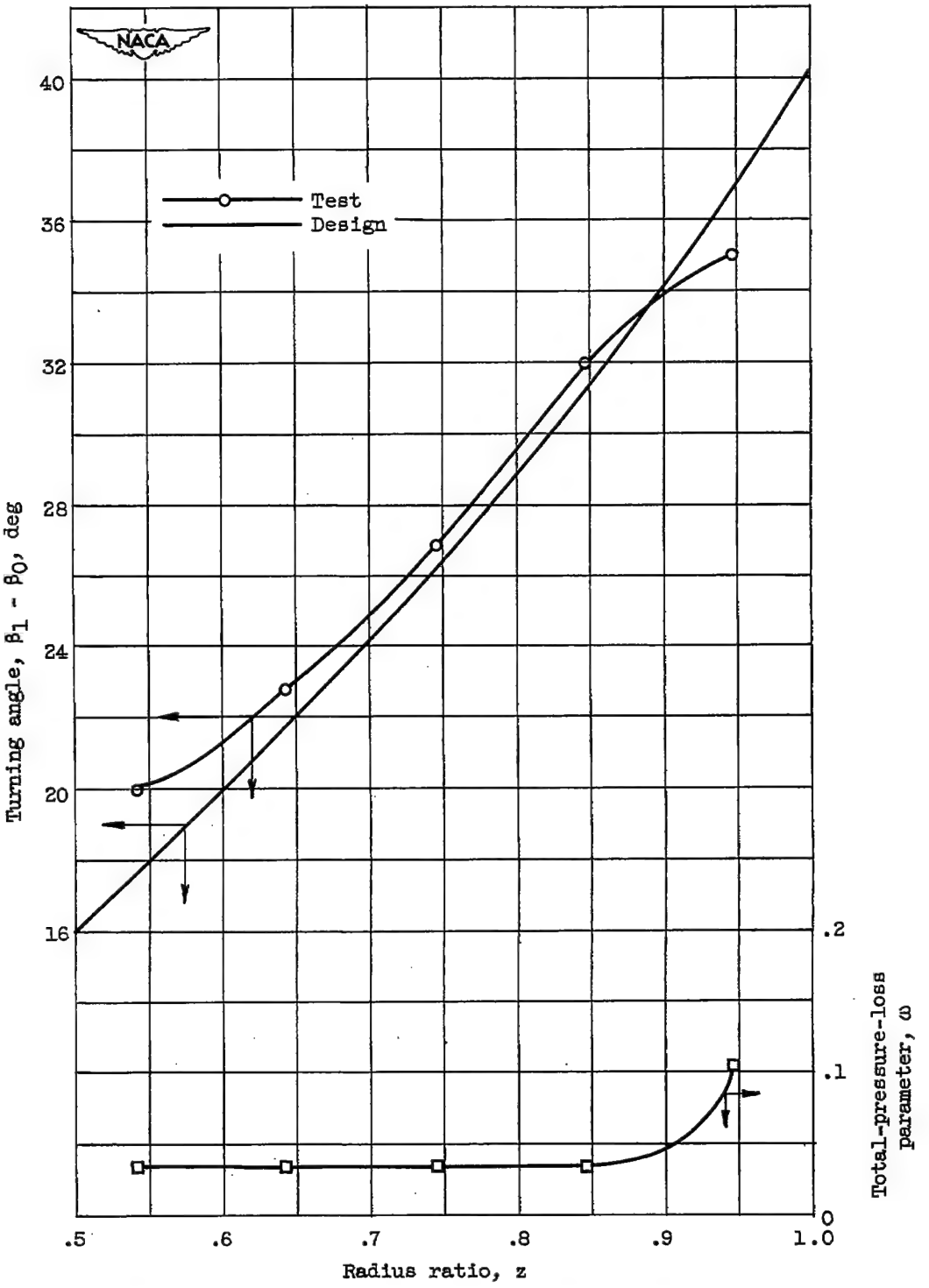

Figure 10. - Variation of total-pressure-loss parameter and turning angle with radius ratio through inlet guide vanes.

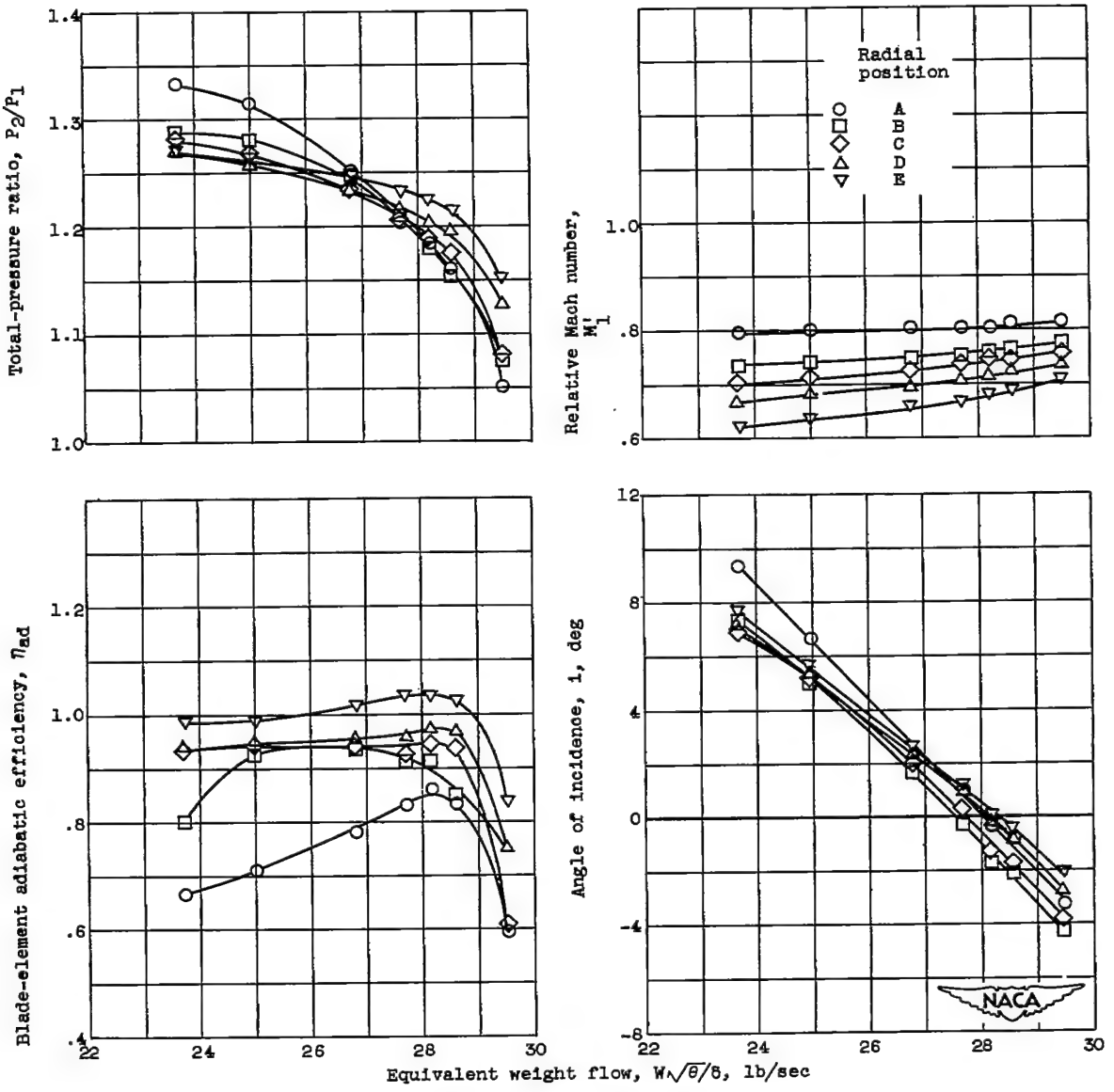

(a) Blade tip speed, 1120 feet per second.

Figure 11. - Blade-element performance data for rotor with guide vanes.

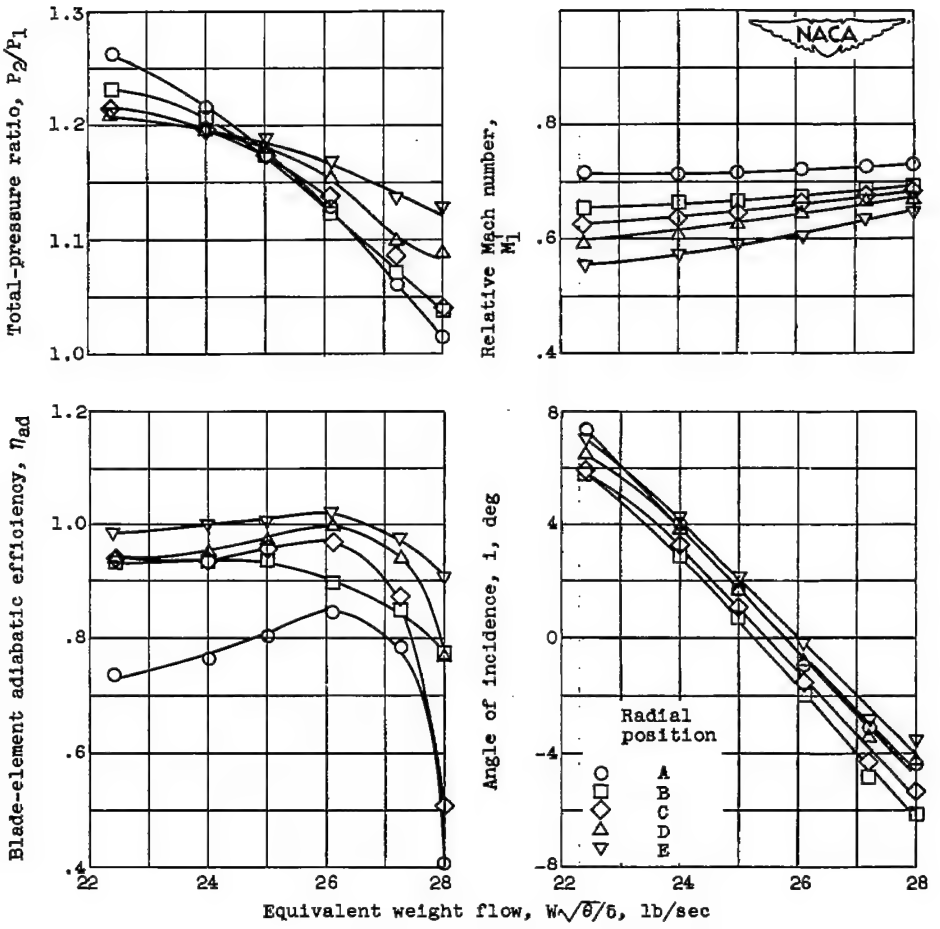

(b) Blade tip speed, 1000 feet per second.

Figure 11. - Continued. Blade-element performance data for rotor with guide vanes.

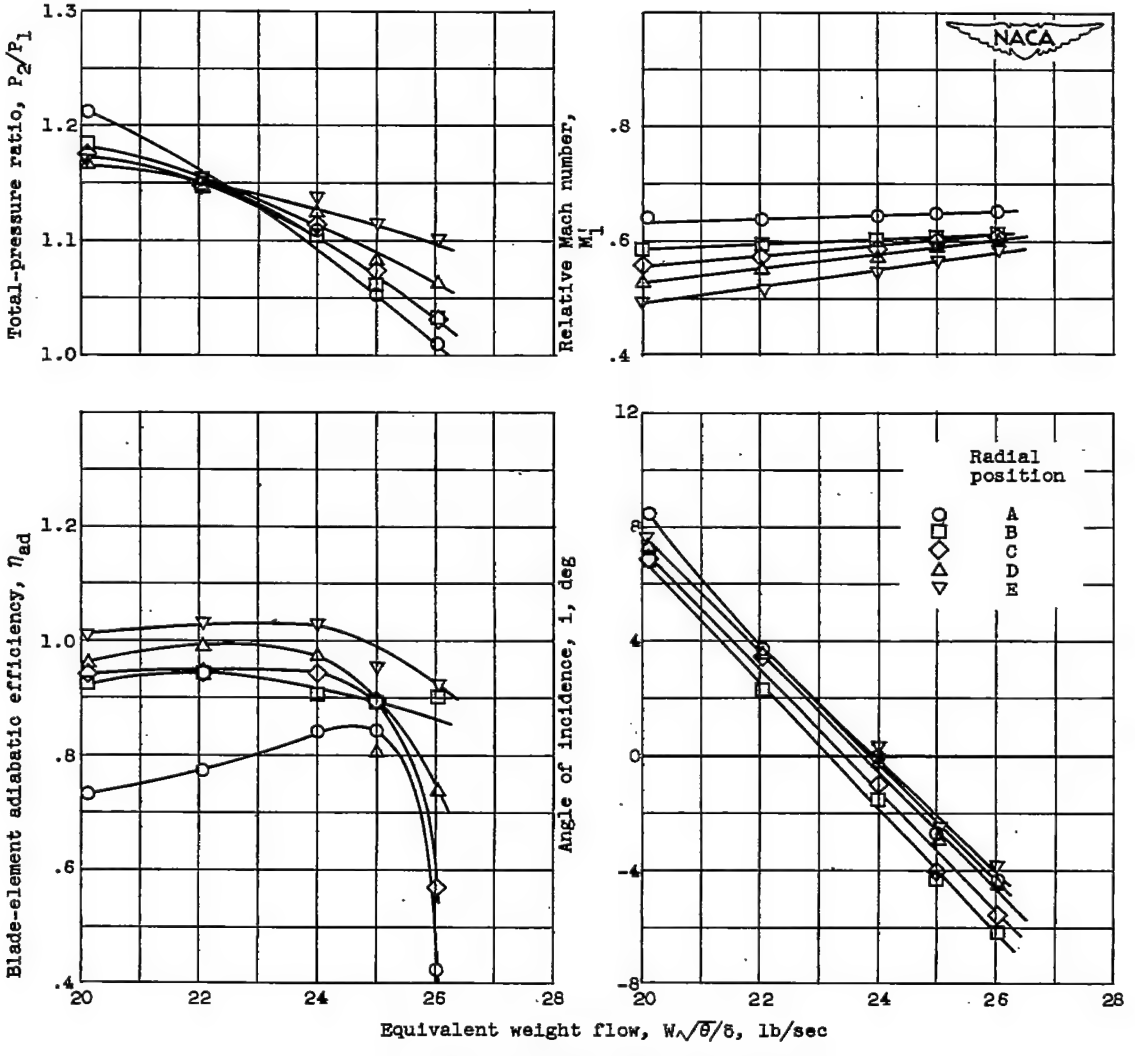

(c) Blade tip speed, 900 feet per second.

Figure 11. - Continued. Blade-element performance data for rotor with guide vanes.

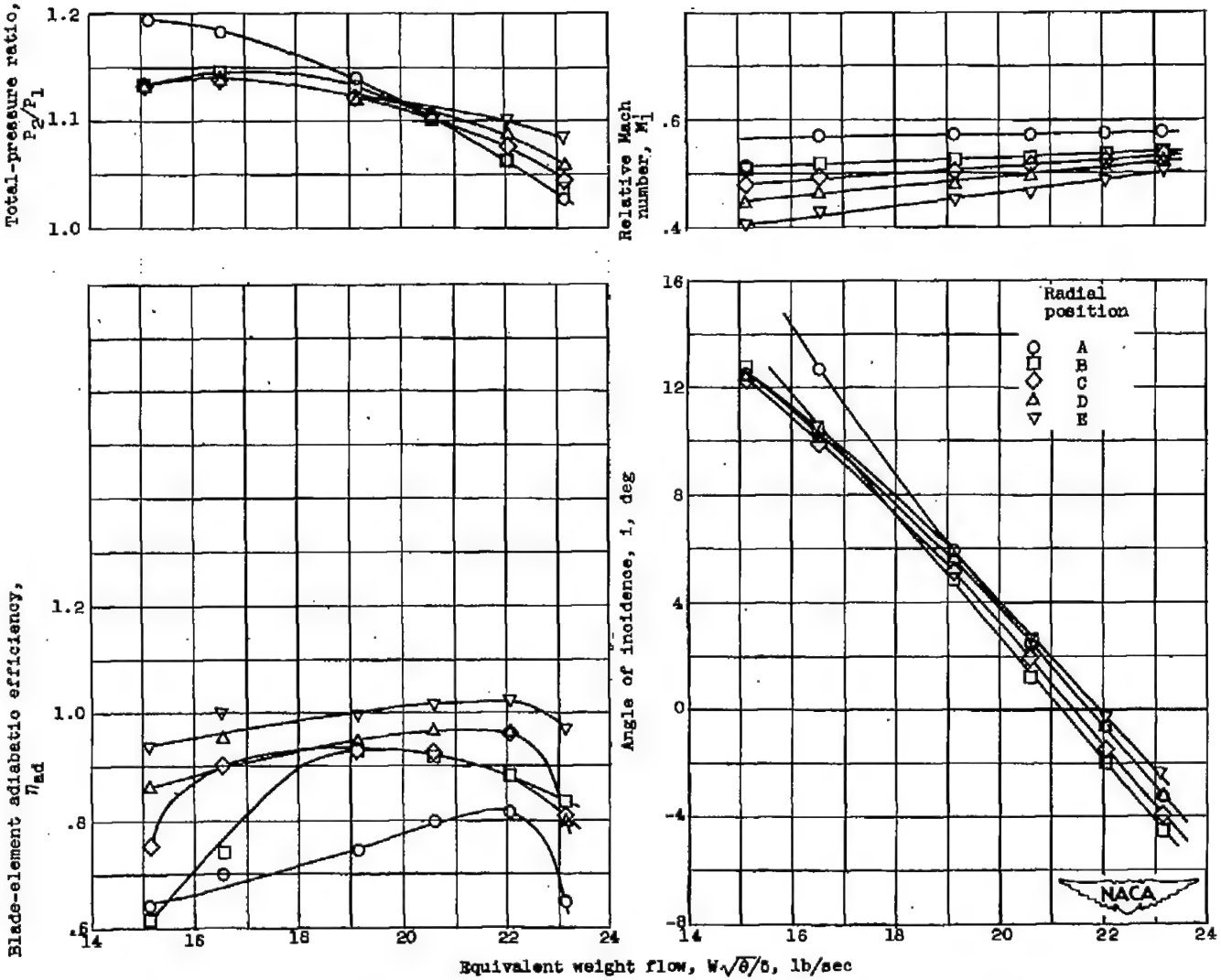

(d) Blade tip speed, 800 feet per second.

Figure 11. - Concluded. Blade-element performance data for rotor with guide vanes.

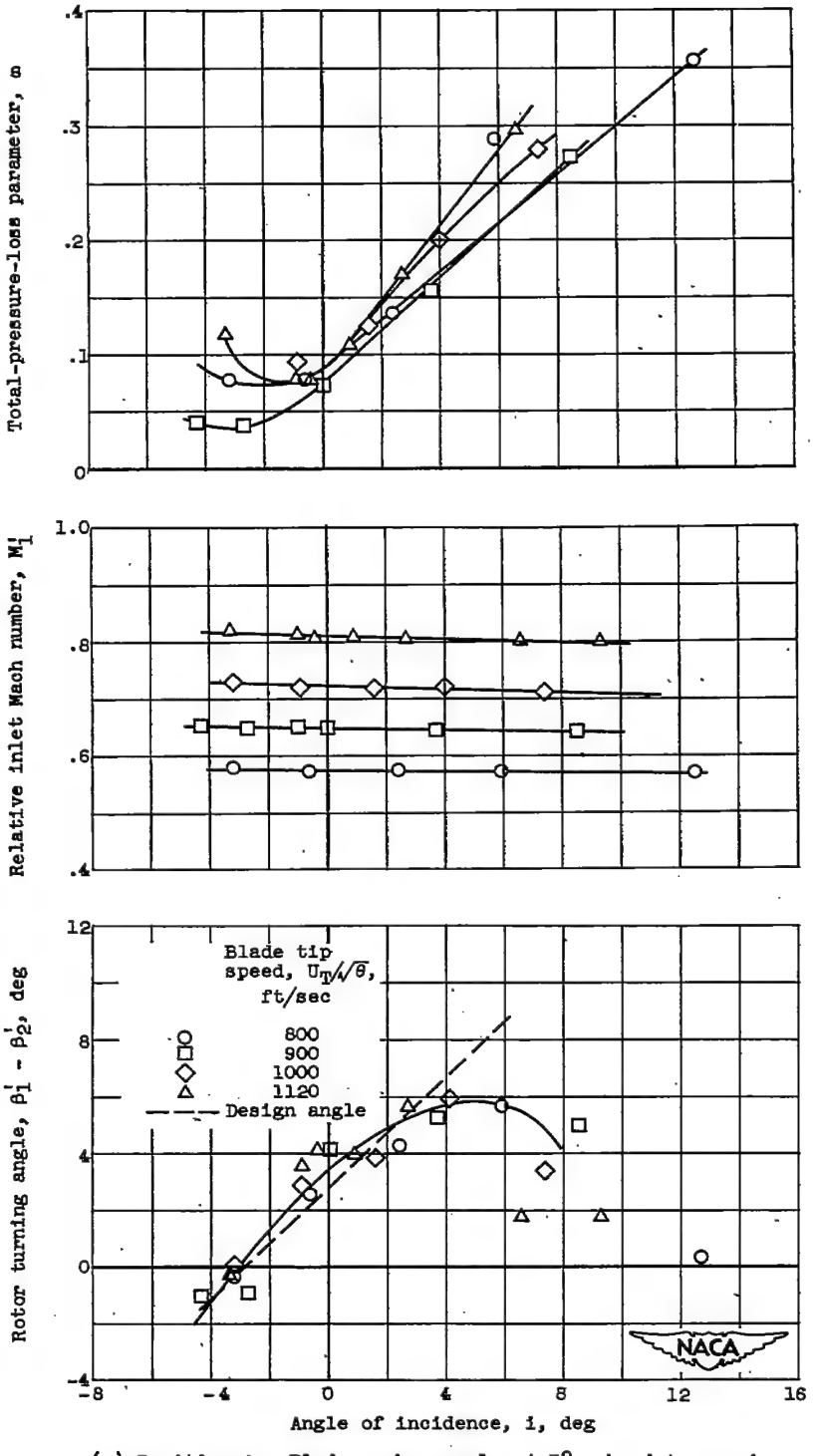

(a) Position A. Blade camber angle, 4.3°; chord-to-spacing ratio, 0.825; blade-setting angle, 51.3°.

Figure 12. - Blade-element performance data at five radial positions for rotor with guide vanes.

[redacted]

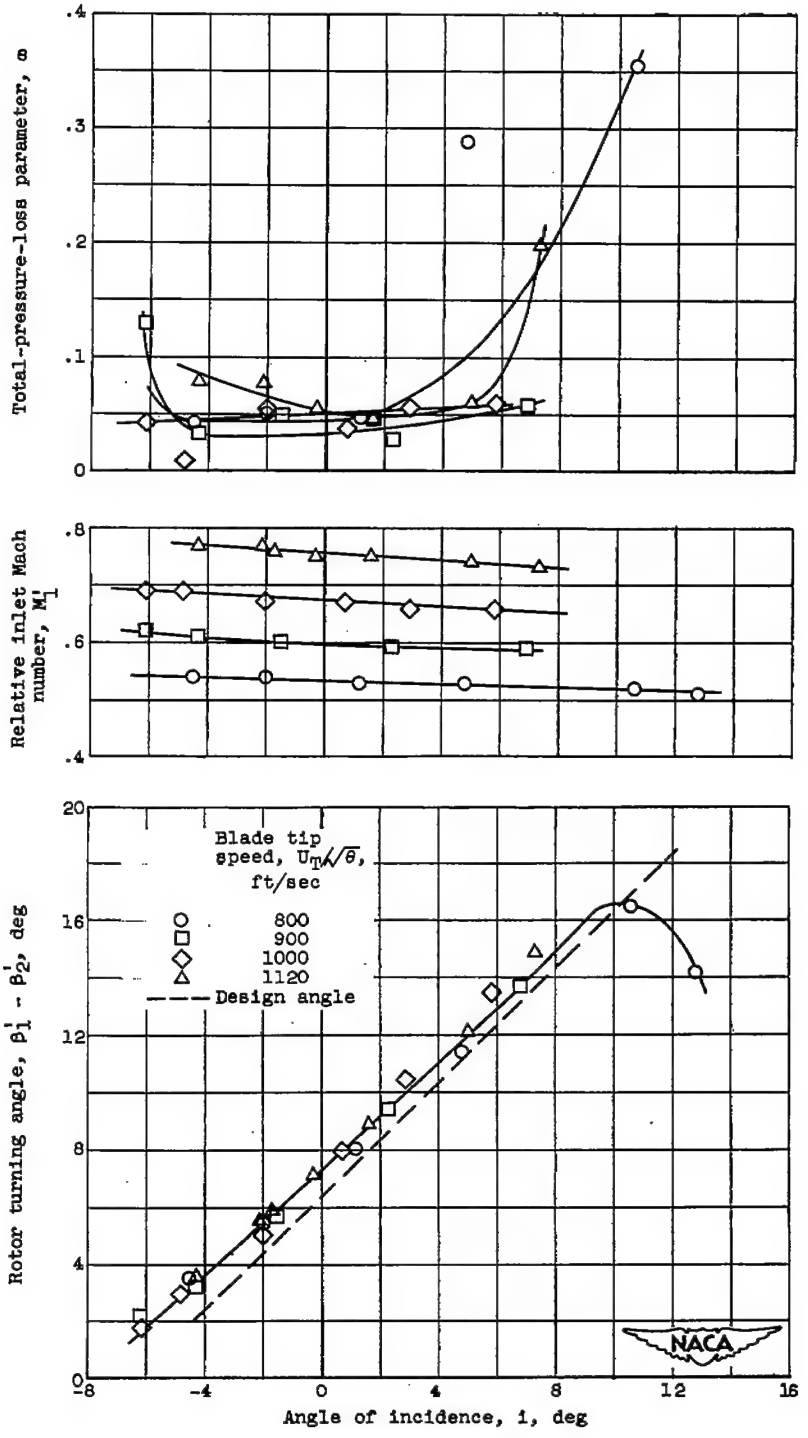

(b) Position B. Blade camber angle, 9.5°; chord-to-spacing ratio, 0.918; blade-setting angle, 43.4°.

Figure 12. - Continued. Blade-element performance data at five radial positions for rotor with guide vanes.

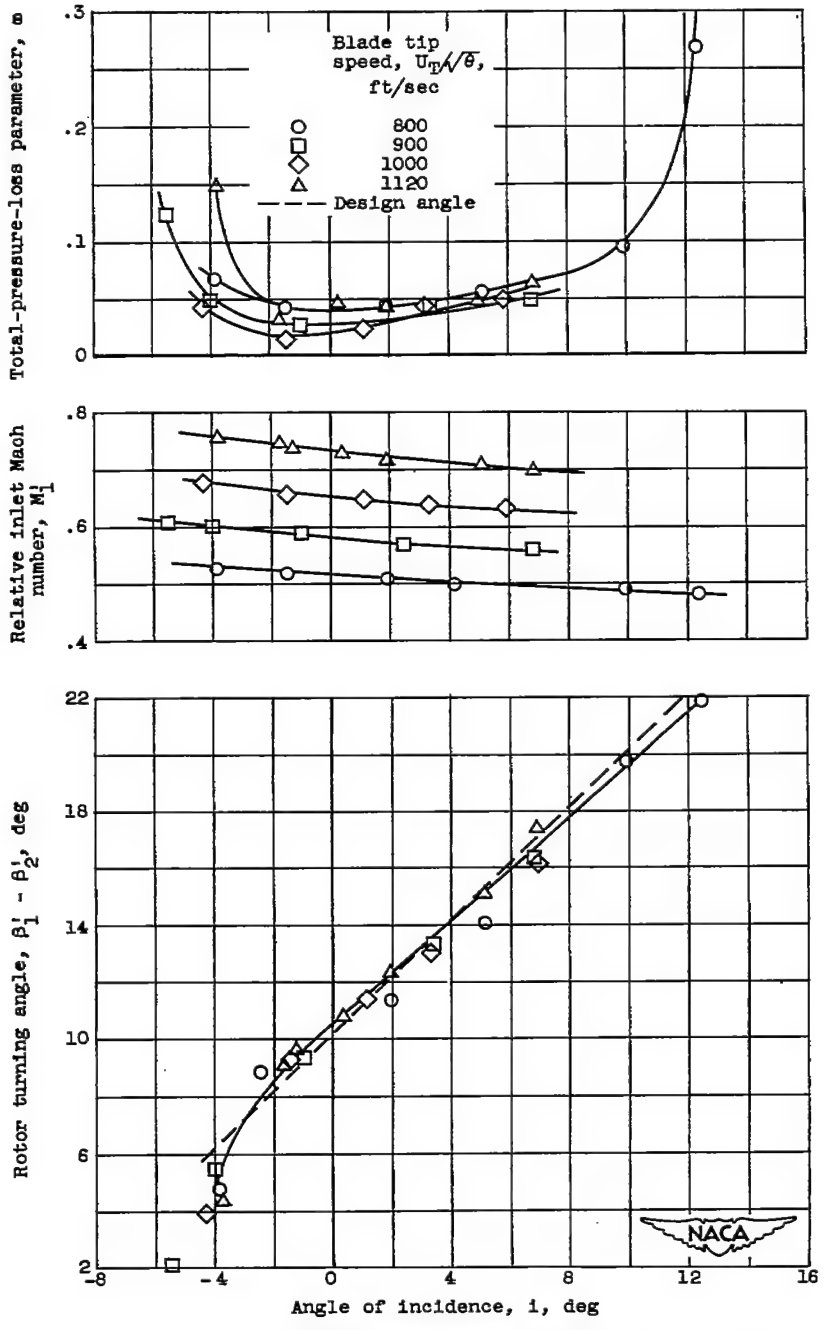

(c) Position C. Blade camber angle, 14.0°; chord-to-spacing ratio, 1.04; blade-setting angle, 34.8°.

Figure 12. - Continued. Blade-element performance data at five radial positions for rotor with guide vanes.

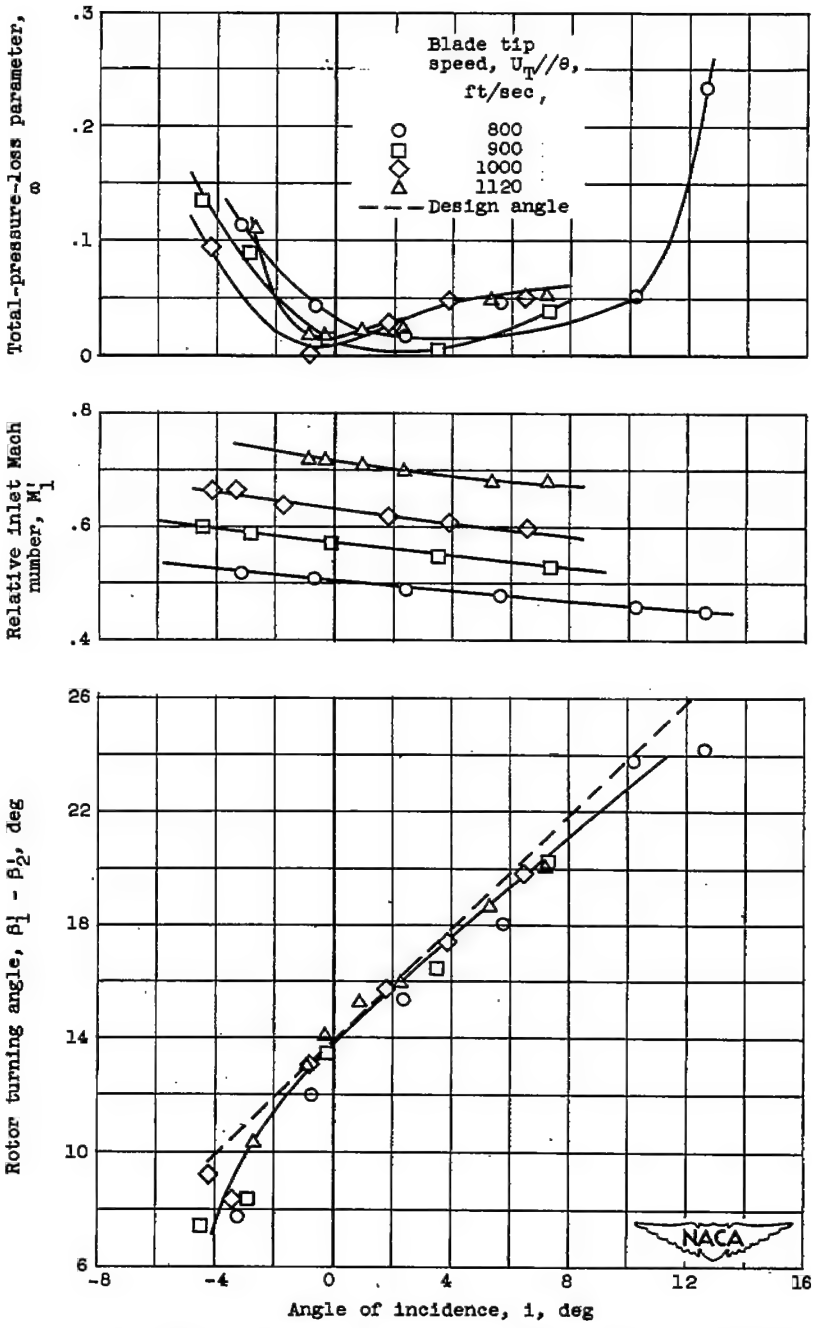

(d) Position D. Blade camber angle, 18.1°; chord-to-spacing ratio, 1.19; blade-setting angle, 26.1°.

Figure 12. - Continued. Blade-element performance data at five radial positions for rotor with guide vanes.

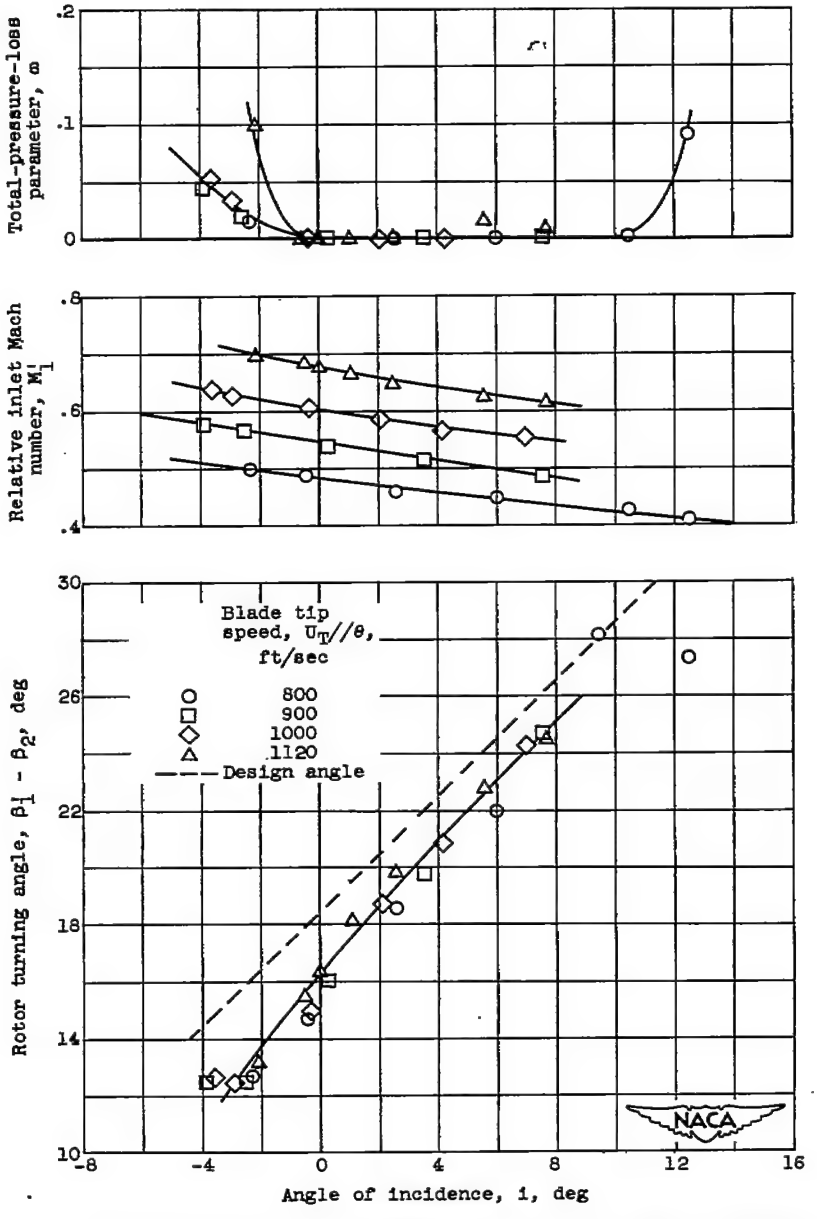

(e) Position E. Blade camber angle, 23.1°; chord-to-spacing ratio, 1.40; blade-setting angle, 17.4°.

Figure 12. - Concluded. Blade-element performance data at five radial positions for rotor with guide vanes.

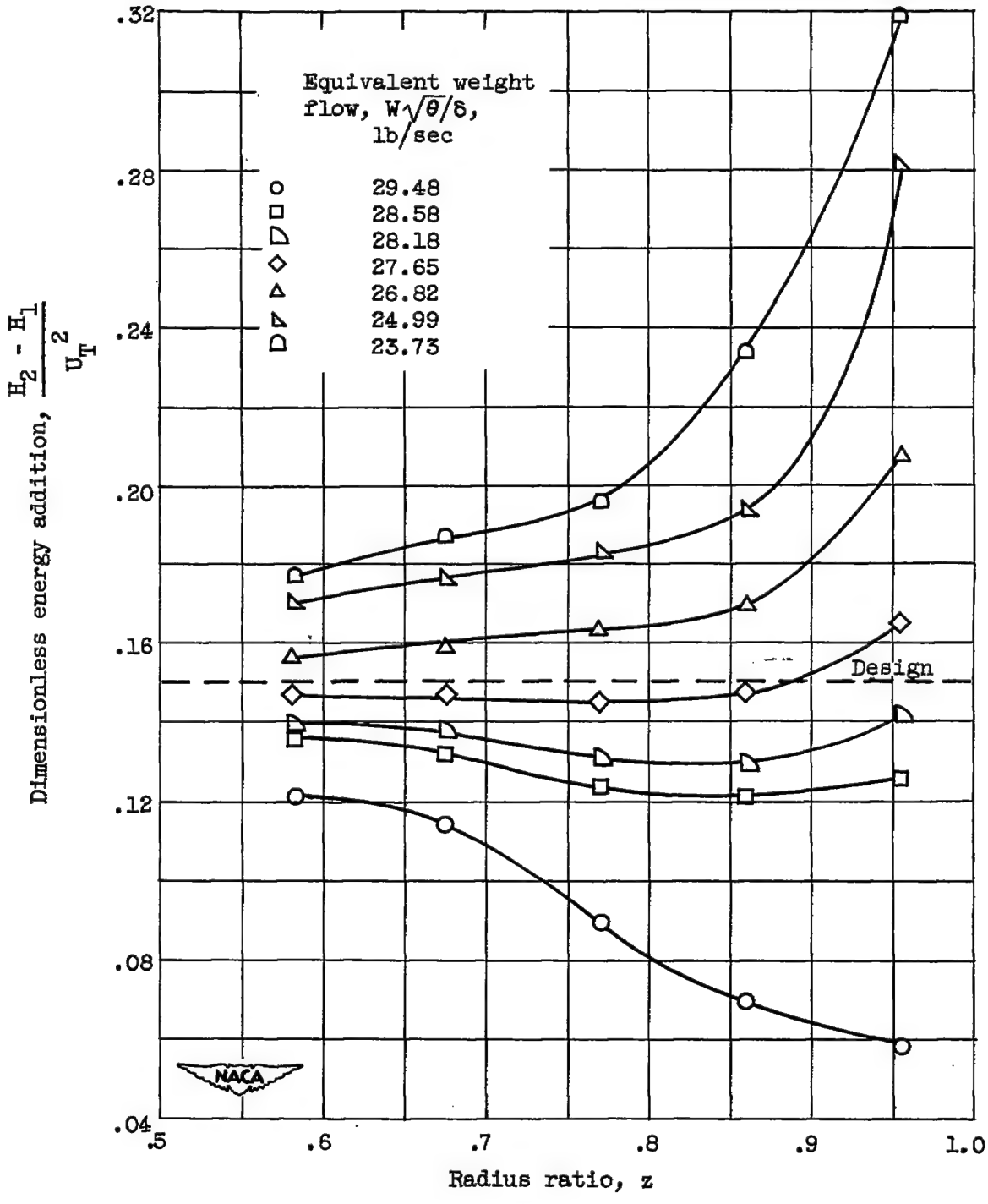

Figure 13. - Dimensionless energy addition plotted against radius ratio at design speed for rotor with guide vanes.

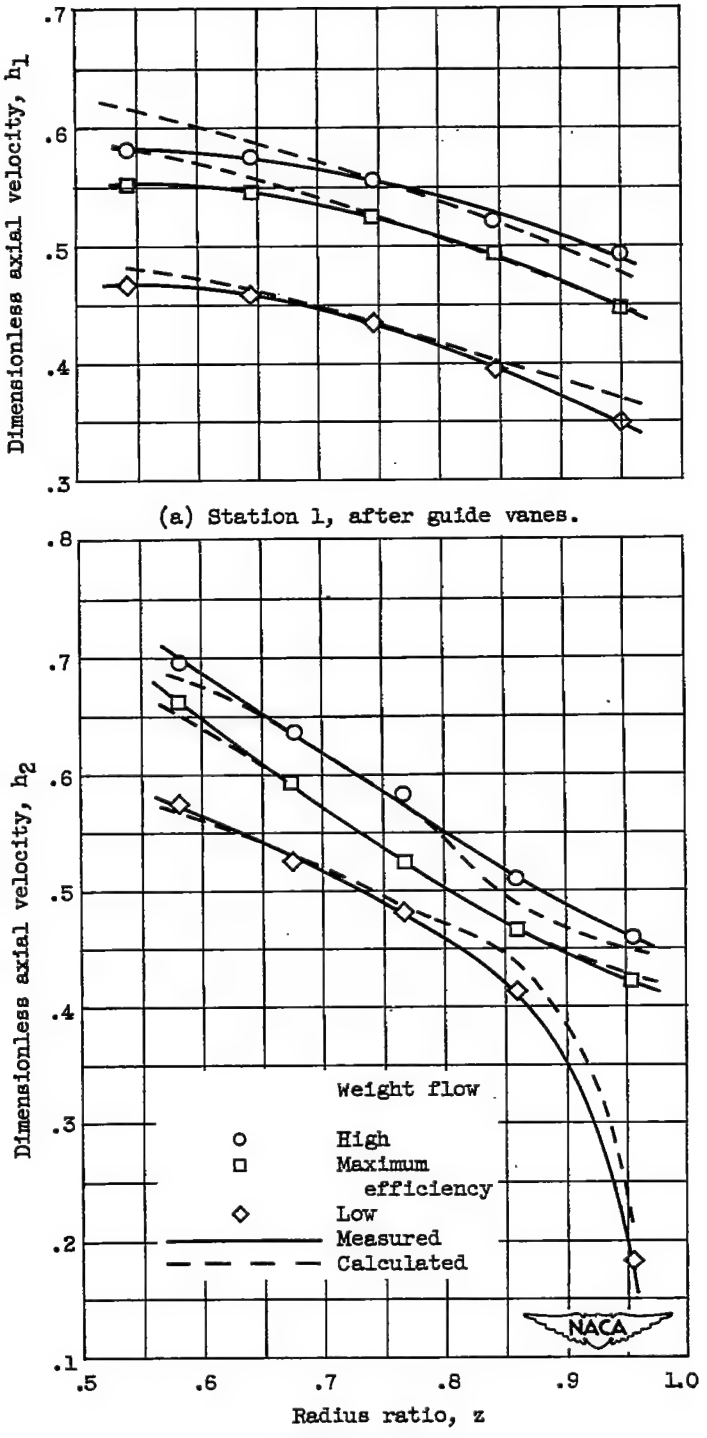

(a) Station 1, after guide vanes.

(b) Station 2, after rotor.

Figure 14. - Measured and calculated dimensionless axial velocity at design speed for rotor with guide vanes.

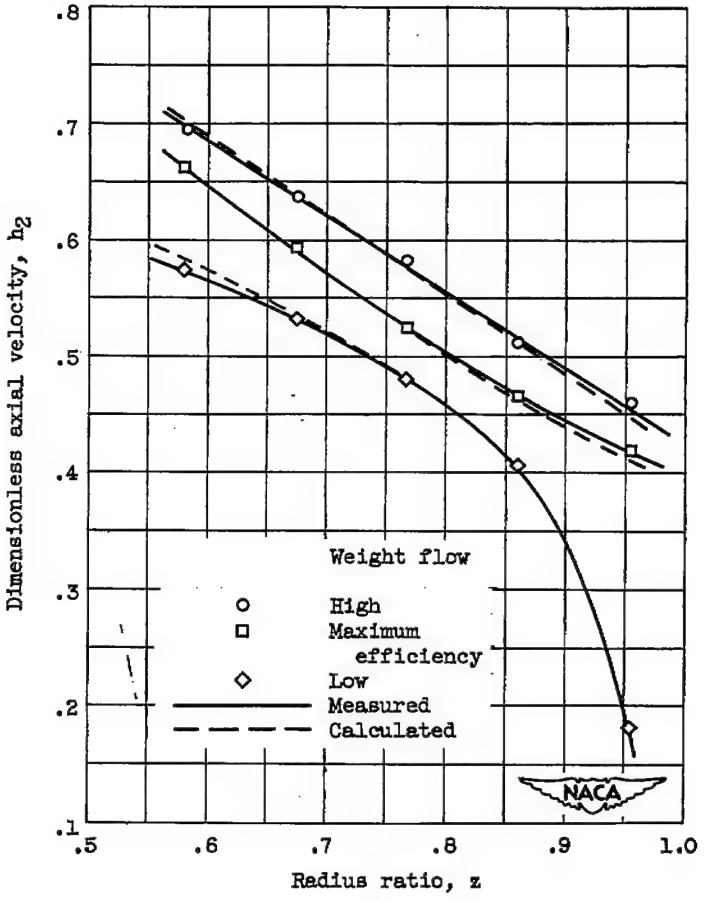

(c) Station 2. Calculated values include entropy-gradient term in radial equilibrium equation.

Figure 14. - Concluded. Measured and calculated dimensionless axial velocity at design speed for rotor with guide vanes.

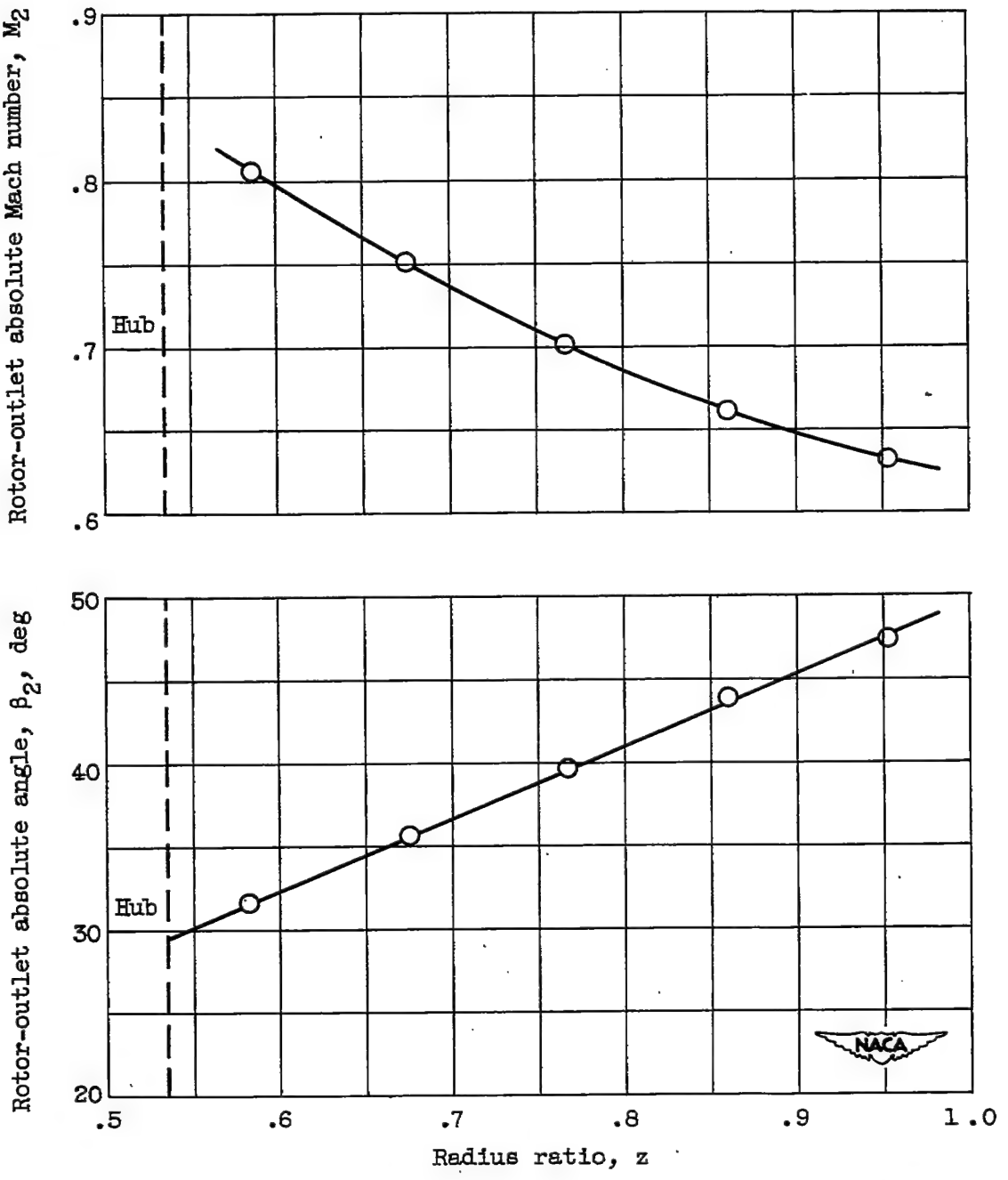

Figure 15. - Rotor-outlet angle and Mach number plotted against radius ratio for rotor with guide vanes. Blade tip speed, 1120 feet per second; equivalent weight flow, 28.18 pounds per second.

[redacted]

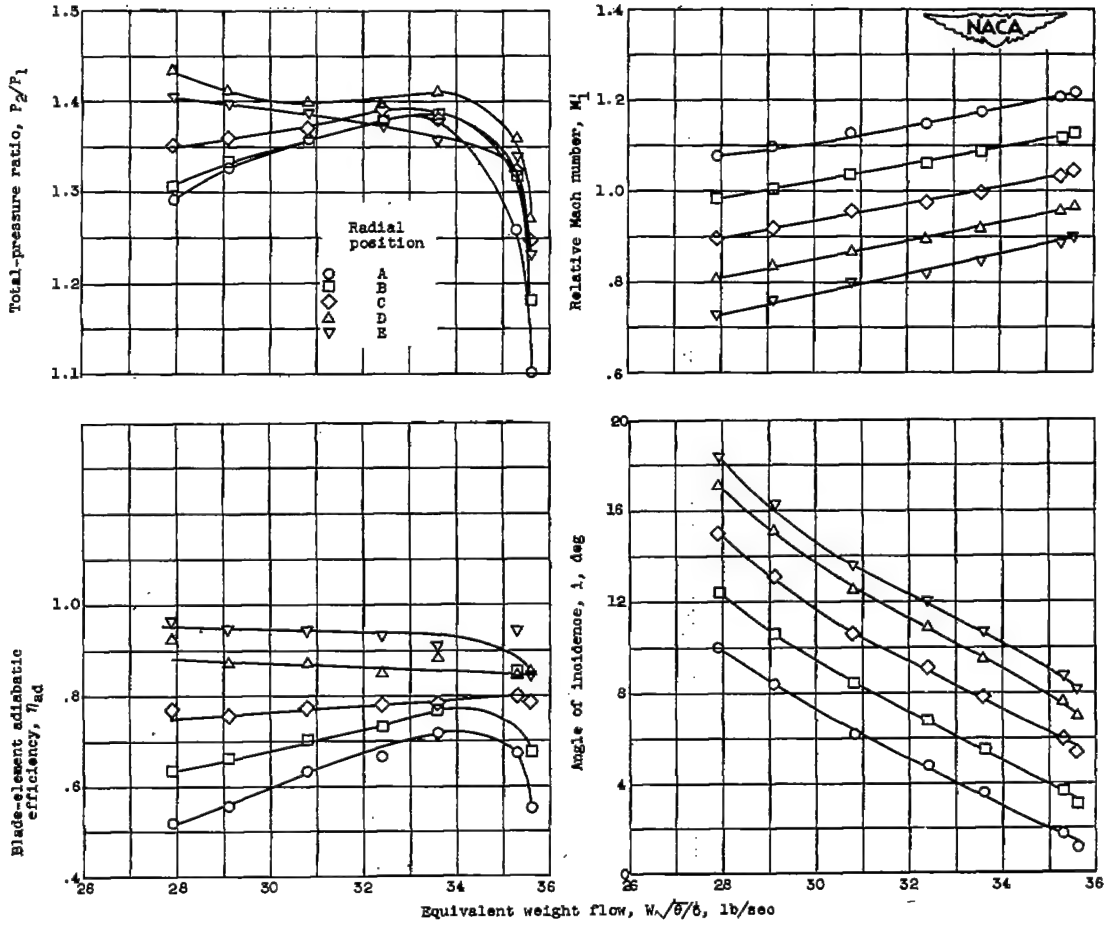

(a) Blade tip speed, 1120 feet per second.

Figure 16. - Blade-element performance data for rotor alone.

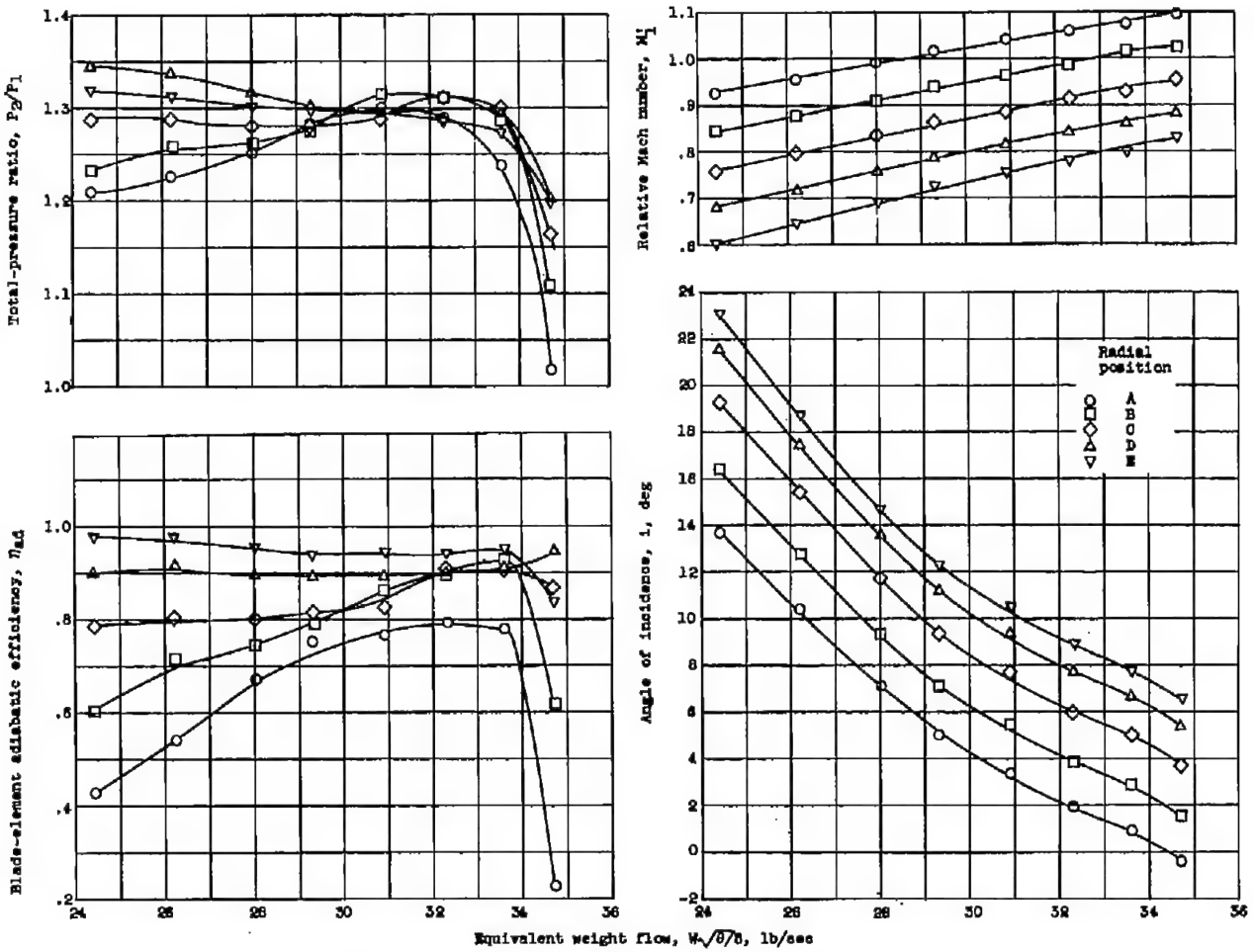

(b) Blade tip speed, 1000 feet per second.

Figure 16. - Continued. Blade-element performance data for rotor alone.

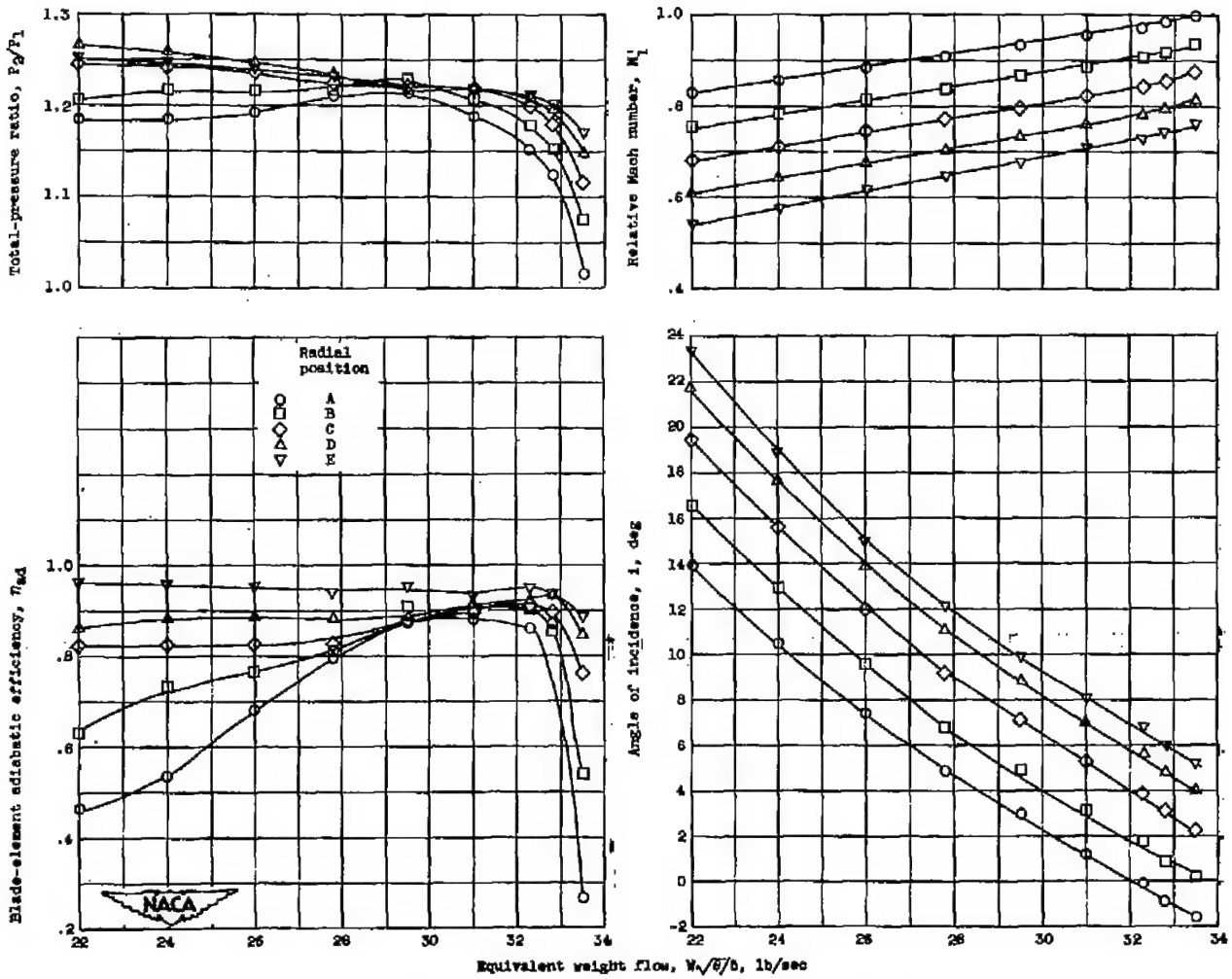

(c) Blade tip speed, 900 feet per second.

Figure 16. - Continued. Blade-element performance data for rotor alone.

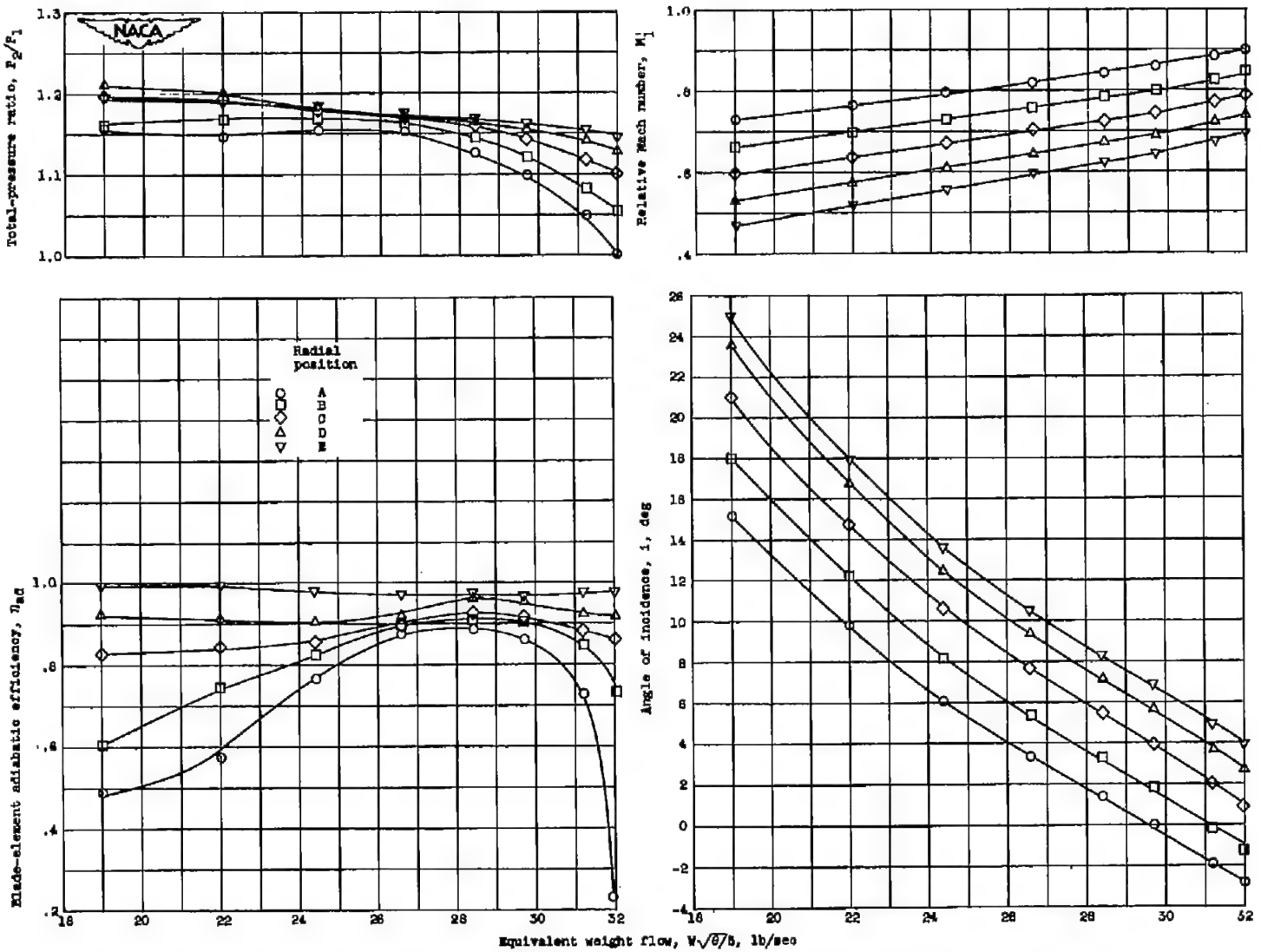

(d) Blade tip speed, 800 feet per second.

Figure 16. - Concluded. Blade-element performance data for rotor alone.

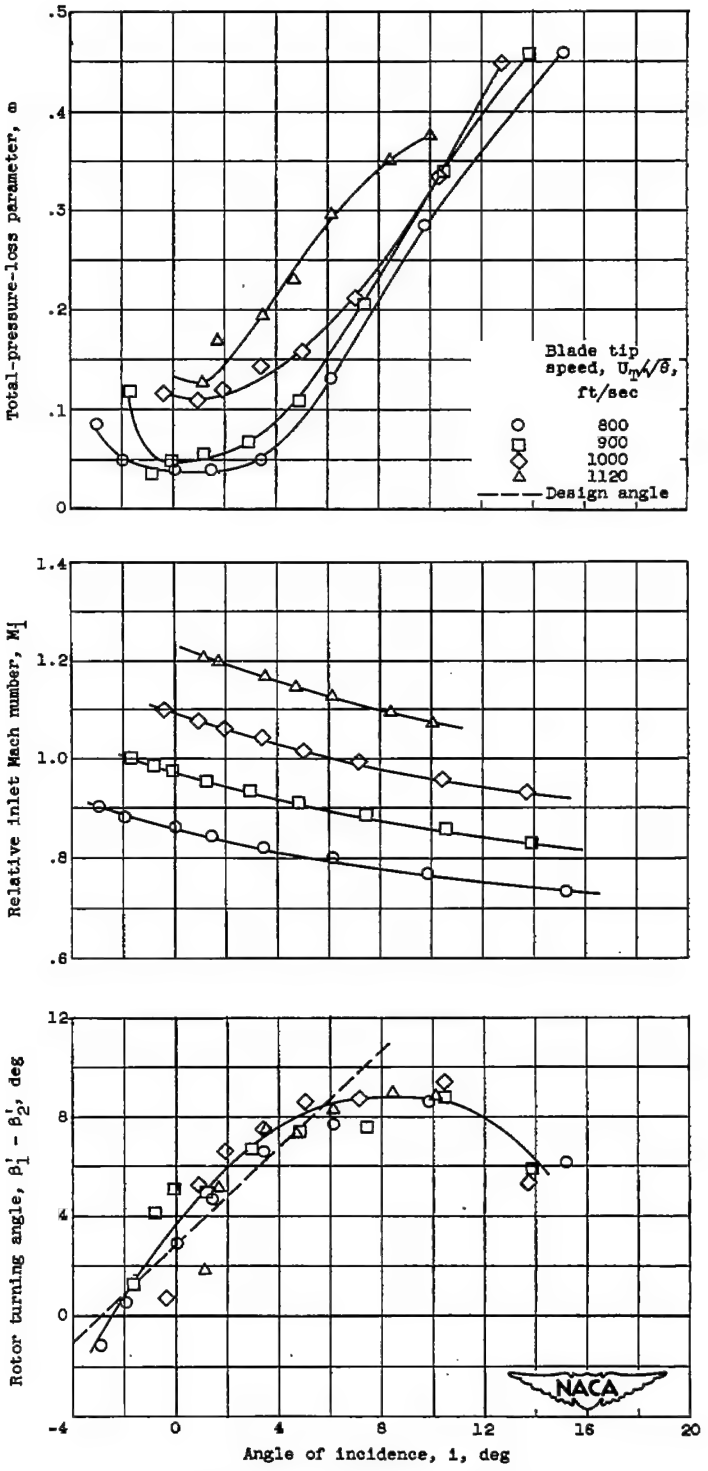

(a) Position A. Blade camber angle, 4.3°; chord-to-spacing ratio, 0.825; blade-setting angle, 51.3°.

Figure 17. - Blade-element performance data at five radial positions for rotor alone.

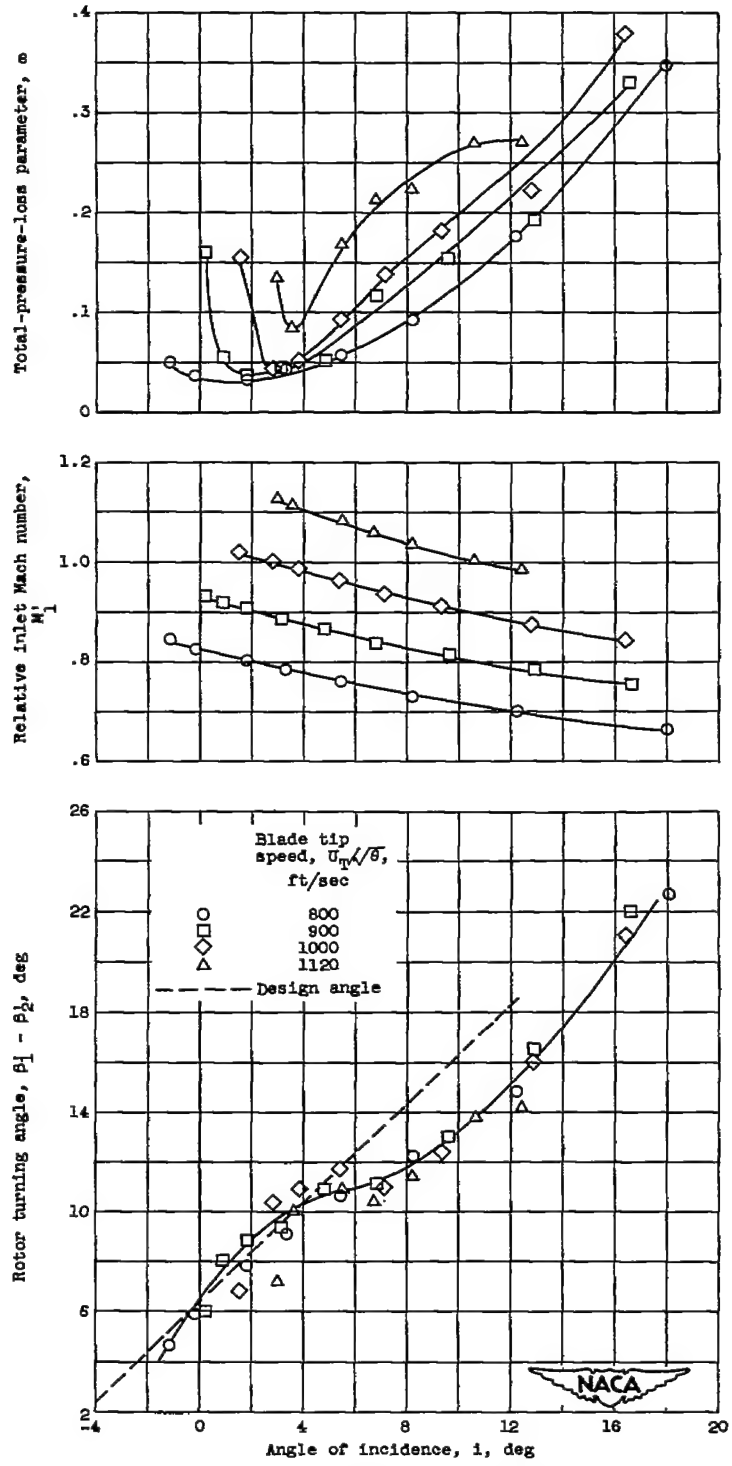

(b) Position B. Blade camber angle, 9.3°; chord-to-spacing ratio, 0.9184; blade-setting angle, 43.4°.

Figure 17. - Continued. Blade-element performance data at five radial positions for rotor alone.

[redacted]

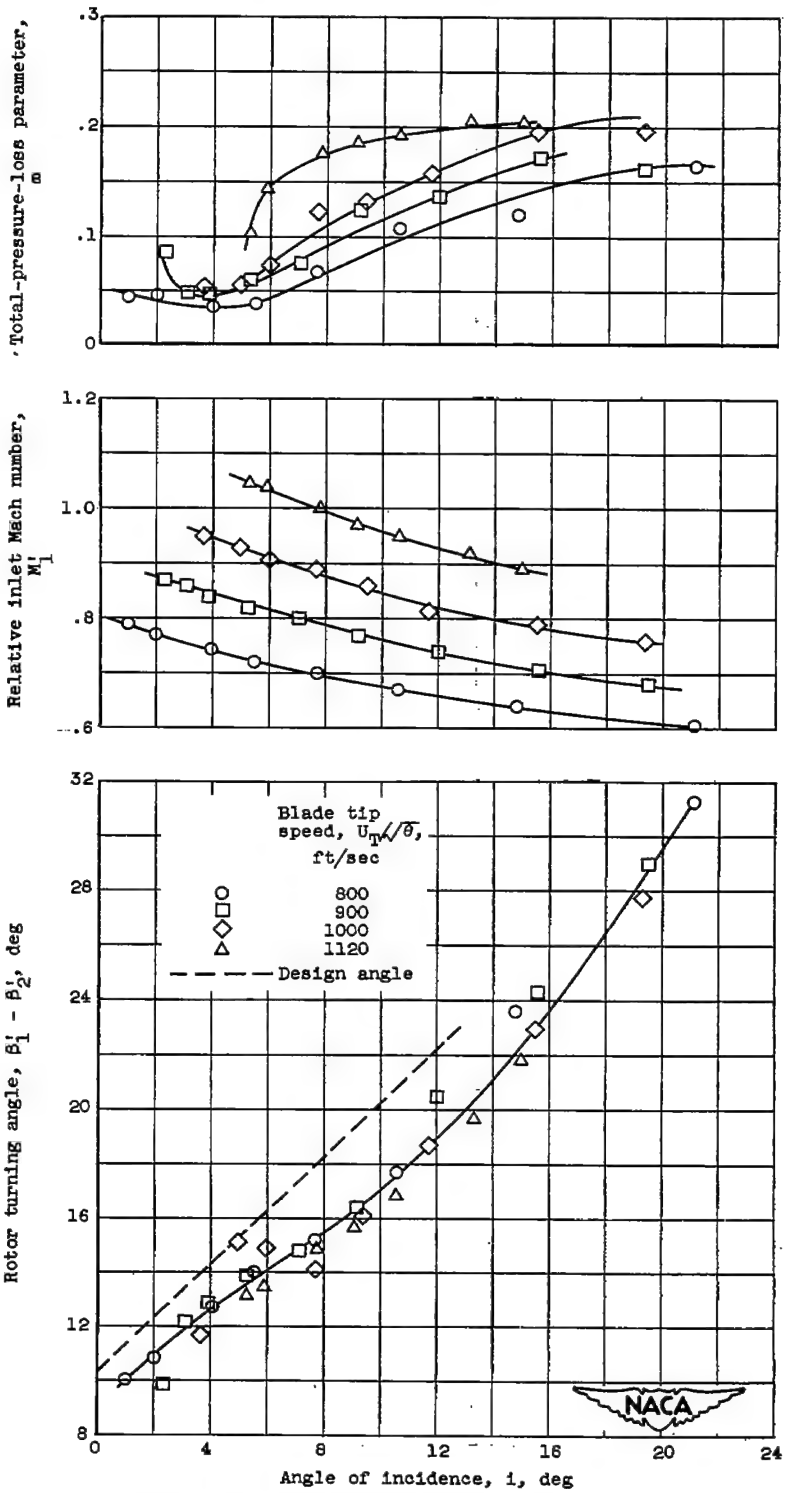

(c) Position C. Blade camber angle, 14.0°; chord-to-spacing ratio, 1.04; blade-setting angle, 34.8°.

Figure 17. - Continued. Blade-element performance data at five radial positions for rotor alone.

[redacted]

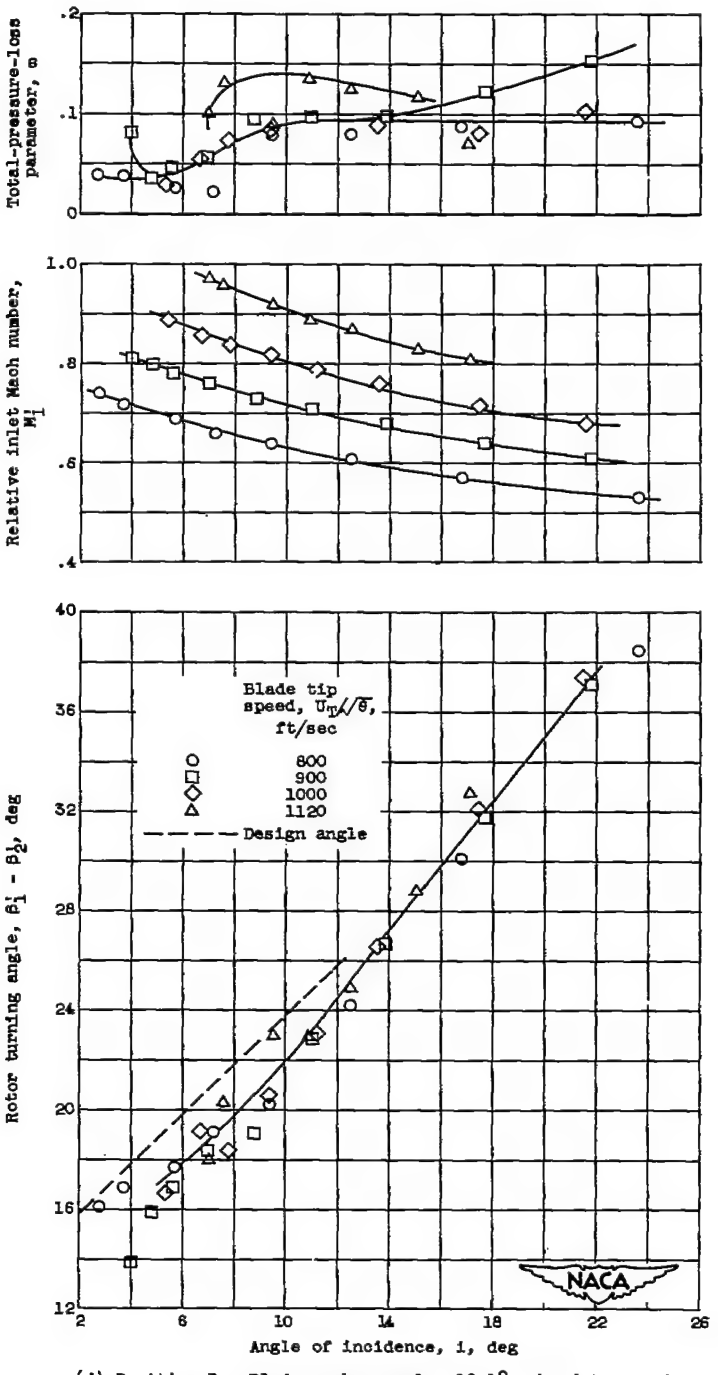

(d) Position D. Blade camber angle, 18.1°; chord-to-spacing ratio, 1.19; blade-setting angle, 26.1°.

Figure 17. - Continued. Blade-element performance data at five radial positions for rotor alone.

[redacted]

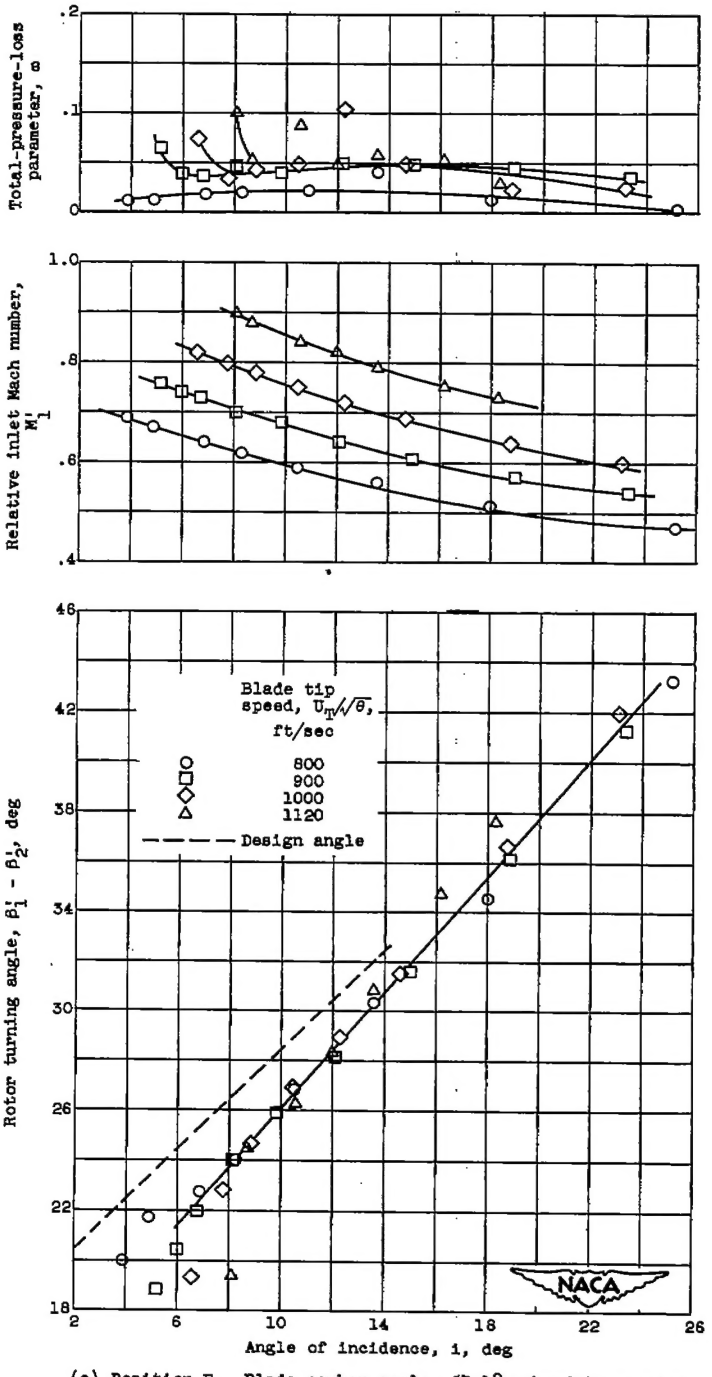

(e) Position E. Blade camber angle, 23.1°; chord-to-spacing ratio, 1.40; blade-setting angle, 17.4°.

Figure 17. - Concluded. Blade-element performance data at five radial positions for rotor alone.

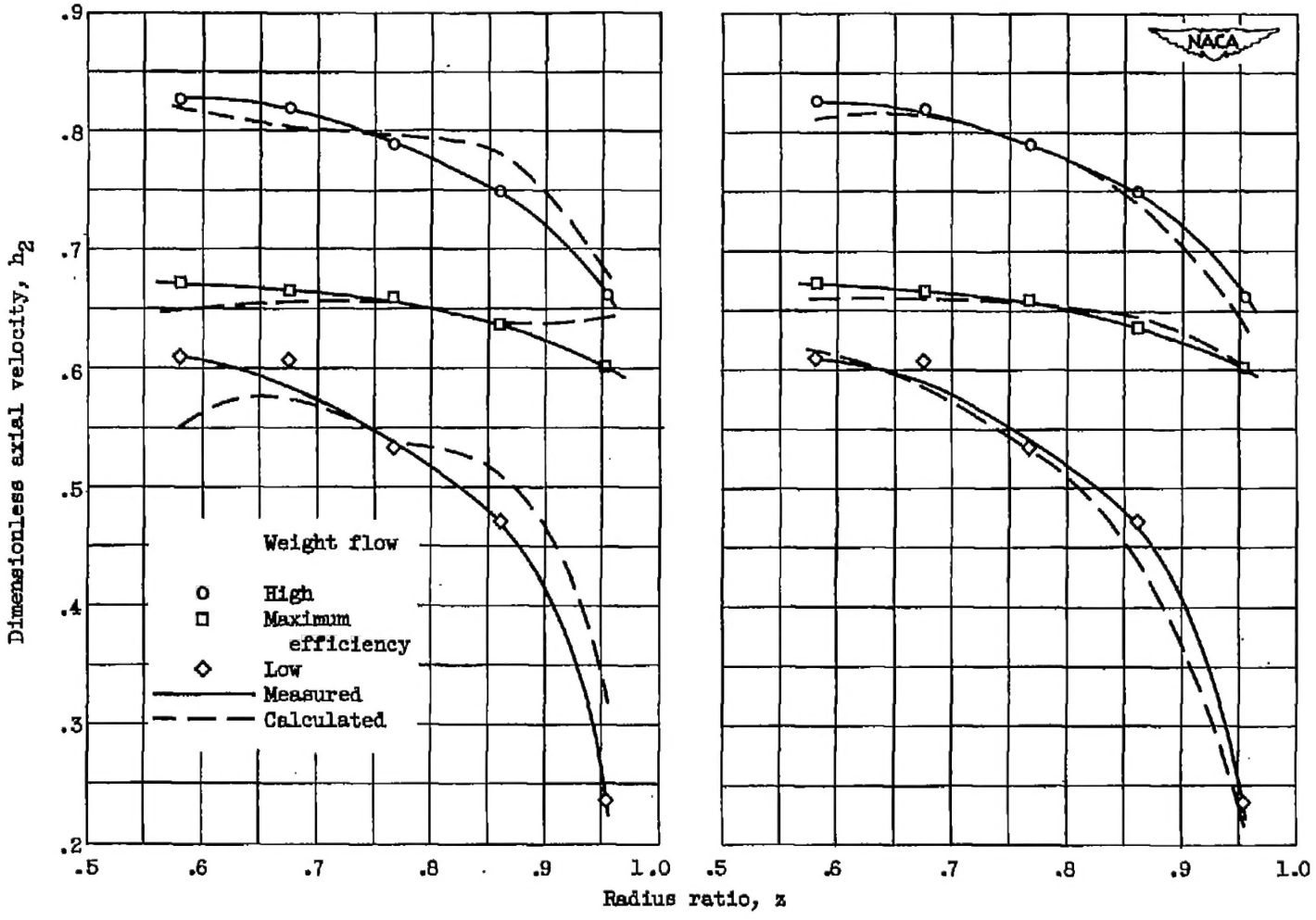

(a) Blade tip speed, 1000 feet per second.

(b) Blade tip speed, 1000 feet per second. Calculated values include entropy-gradient term in radial-equilibrium equation.

Figure 18. - Measured and calculated dimensionless axial velocity at station 2 for rotor alone.

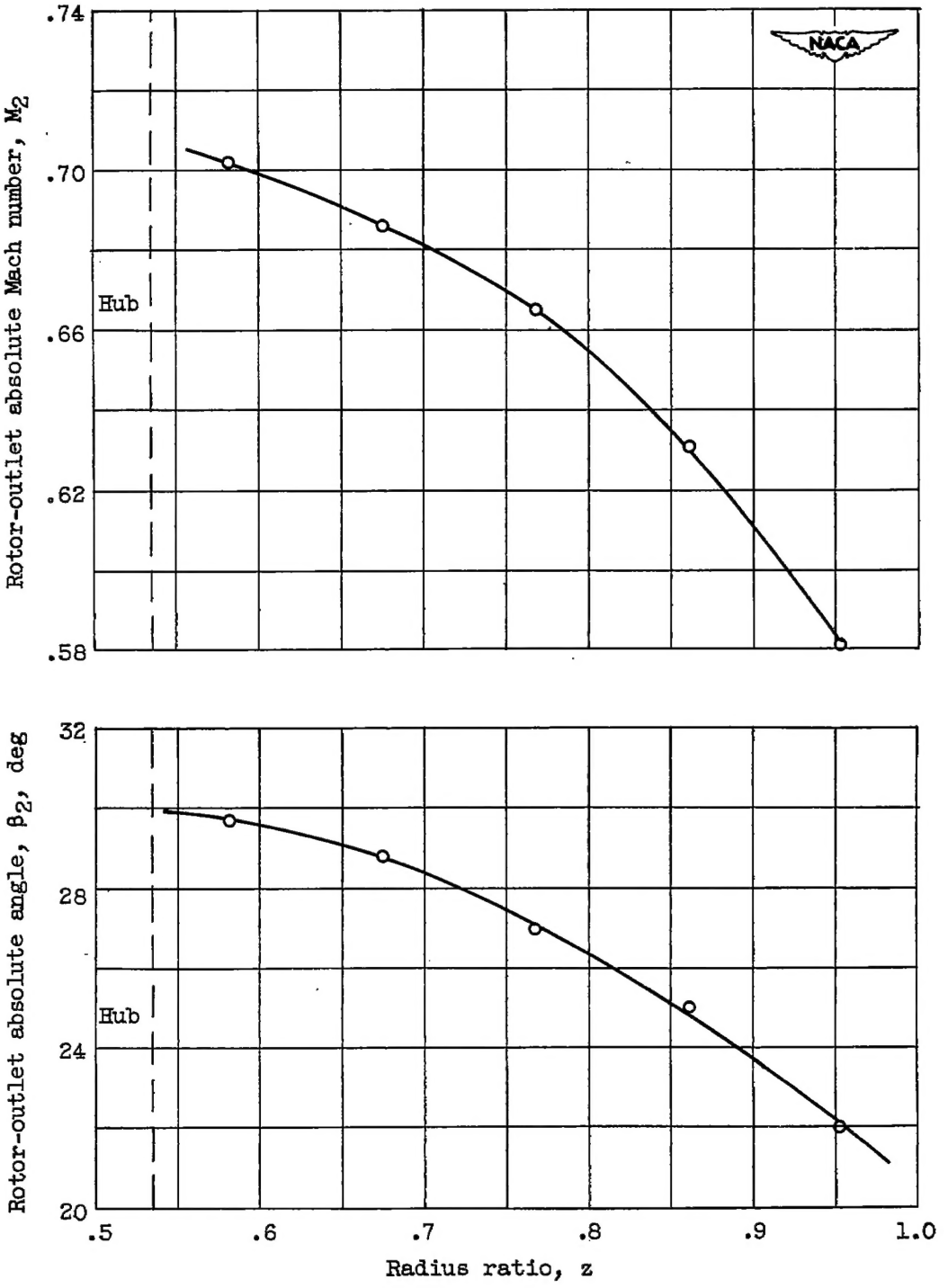

Figure 19. - Rotor-outlet angle and Mach number plotted against radius ratio for rotor alone. Blade tip speed, 1000 feet per second; equivalent weight flow, 33.58 pounds per second.

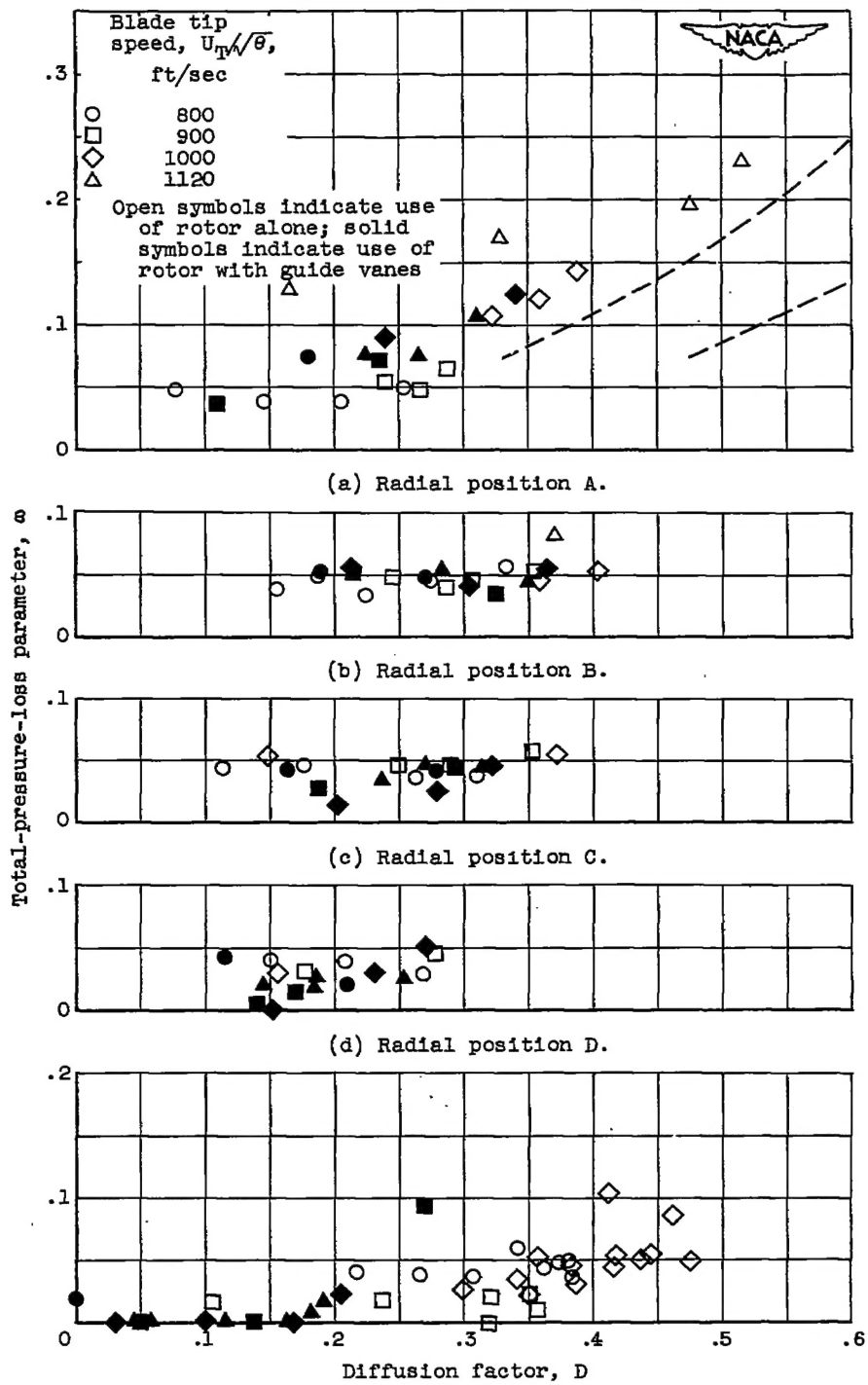

(a) Radial position A.

(b) Radial position B.

(c) Radial position C.

(d) Radial position D.

(e) Radial position E.

Figure 20. - Variation of total-pressure-loss parameter with diffusion factor for points near optimum incidence angle.

NACA-Langley - 7-3-53 - 400